Adaptation, not prediction, drives neuronal spiking responses in mammalian sensory cortex

Jacob A. Westerberg[1,2,*], Yihan S. Xiong[1,*], Hamed Nejat[1], Eli Sennesh[1], Séverine Durand[3], Ben Hardcastle[3], Hannah Cabasco[3], Hannah Belski[3], Ahad Bawany[3], Ryan Gillis[3], Henry Loeffler[3], Carter R. Peene[3], Warren Han[3], Katrina Nguyen[3], Vivian Ha[3], Tye Johnson[3], Conor Grasso[3], Ahrial Young[3], Jackie Swapp[3], Ben Ouellette[3], Shiella Caldejon[3], Ali Williford[3], Peter A. Groblewski[3], Shawn R. Olsen[3], Carly Kiselycznyk[3], Jerome A. Lecoq[3], Alexander Maier[1], and André M. Bastos[1,†]

[1]*Department of Psychology, Vanderbilt Brain Institute, Vanderbilt Vision Research Center, Vanderbilt University, Nashville, Tennessee, United States*
[2]*Department of Vision and Cognition, Netherlands Institute for Neuroscience, Royal Netherlands Academy of Arts and Sciences, Amsterdam, The Netherlands*
[3]*Allen Institute for Brain Science, Seattle, Washington, United States.*

[†]Correspondence: andre.bastos@vanderbilt.edu
[*]These authors contributed equally

ORCiD:

J.A.W.	- 0000-0001-5331-8707	C.R.P.	- 0009-0000-6660-2264	B.O.	- 0000-0003-4913-554X
Y.S.X.	- 0009-0007-1298-3672	W.H.	- 0009-0006-0104-0380	A.W.	- 0009-0000-7282-7515
H.N.	- 0009-0003-5963-5801	K.N.	- 0009-0009-8547-9703	P.A.G.	- 0000-0002-8415-1118
E.S.	- 0000-0001-7014-8471	V.H.	- 0009-0005-0093-3825	S.R.O.	- 0000-0002-9568-7057
S.D.	- 0000-0001-7788-0200	T.J.	- 0009-0006-7239-7571	C.K.	- 0009-0006-8410-1192
H.C.	- 0009-0001-7899-2463	C.G.	- 0009-0003-6384-4075	J.A.L.	- 0000-0002-0131-0938
H.B.	- 0009-0001-5422-5964	B.H.	- 0000-0002-4819-5631	A.M.	- 0000-0002-7250-502X
H.L.	- 0009-0007-3935-6863	J.S.	- 0009-0008-4965-6242	A.M.B.	- 0000-0003-1804-4418
A.B.	- 0009-0002-5495-5411	R.G.	- 0009-0000-1879-6519		

Summary

Predictive coding (PC) hypothesizes that the brain computes internal models of predicted events and that unpredicted stimuli are signaled with prediction errors that feed forward. We tested this hypothesis using a visual oddball task. A repetitive sequence interrupted by a novel stimulus is a “local” oddball. “Global” oddballs defy predictions while repeating the local context, thereby dissociating genuine prediction errors from adaptation-related responses. We recorded neuronal spiking activity across the visual hierarchy in mice and monkeys viewing these oddballs. Local oddball responses largely followed PC: they were robust, emerged early in layers 2/3, and fed forward. Global oddball responses challenged PC: they were weak, absent in most visual areas, more robust in prefrontal cortex, emerged in non-granular layers, and did not involve inhibitory interneurons relaying predictive suppression. Contrary to PC, genuine predictive coding does not emerge early in sensory processing, and is instead exclusive to more cognitive, higher-order areas.

Keywords

Cognition, Predictive Coding, Macaque, Mouse, Oddball, Optogenetics, Perception, Visual Cortex

Highlights

- Core principles of Predictive Coding explain local, but not global oddball brain responses
- Global oddballs are sparsely encoded in visual cortex and do not engage feedforward mechanisms
- Parvalbumin and somatostatin interneurons do not support sensory global oddball detection
- Global oddballs are earliest, and most robustly encoded, in prefrontal brain areas

Significance

Global oddballs defy our expectations without standing out from their local context. Whether they are encoded in sensory brain areas was uncertain. Through multiarea neurophysiological recordings in mice and monkeys, Westerberg et al. show that global oddballs neuronal responses contradicts predictive coding hypotheses and emerge in higher order areas.

Introduction

Predictions shape our perception and it is often immediately recognizable when our predictions are violated (Itti and Baldi, 2009). Predictive coding (PC) has emerged as one popular theoretical framework to explain how predictions are instantiated in the brain (Friston, 2010; Rao and Ballard, 1999). One likely reason for the appeal of PC is its wide explanatory power despite its simplicity: less than a handful of theoretical constructs (prior probabilities/predictions, incoming data, prediction errors) account for a large host of neurophysiological and psychological phenomena. These phenomena range from the mismatch negativity (Garrido et al., 2007), sensory processing (Schwiedrzik and Freiwald, 2017), and adaptation (Hosoya et al., 2005) to attentional modulation (Brown and Friston, 2013; Kok et al., 2011; Smout et al., 2019; Spratling, 2008). It has even been proposed that PC models can be a building block to understand conscious experience (Seth et al., 2012).

Predictive coding (PC) models make a series of hypotheses (schematized in Figure 1A) about the nature and underlying mechanisms of neuronal processing (Bastos et al., 2012; Friston, 2005; Friston et al., 2017; Keller and Mrsic-Flogel, 2018; Rao and Ballard, 1999; Schultz et al., 1997; Spratling, 2010; Srinivasan et al., 1982). Specifically, PC proposes that the brain compares incoming sensory information against a prediction signal. This prediction is based on an internal model about the statistics of the environment; these statistics are typically taken to include the mean expected stimulus (typically denoted mathematically as μ) and the precision of the expected stimulus (typically denoted mathematically as Π). Predictions are transmitted to sensory areas, and if an incoming sensory signal matches the prediction, the two signals cancel. Thus, expected sensory data are “explained away” and leave the brain unexcited. In other words, PC is subtractive and multiplicative: when sensory signals do not match the prediction, subtraction results in a larger value, called the prediction error, which is weighted by the precision. This error signal has been proposed to be computed in superficial layers 2 and 3 of sensory cortex, which propagate the signal in the feedforward direction, up the cortical hierarchy (Bastos et al., 2012). Being a second-order statistic, the precision Π is always a positive, nonzero quantity, ensuring that prediction errors are fed up the cortical hierarchy, even if attenuated. As they ascend, prediction errors instigate updates to the internal model to improve predictions, and associated prediction update signals flow back down the hierarchy.

PC has also been proposed to occur over a series of computational steps, each of which compares predictions to prediction errors from a previous step (Rao and Ballard, 1999). This “hierarchical predictive coding model” has since been further modified to fit both the structural and functional architecture of the neocortex (Bastos et al., 2012; Friston, 2010) (Figure 1A). These hierarchical models efficiently predict and explain the cortical responses to first order pattern violations (“local oddballs”), such as a change from repeated stimulation (e.g., a stimulus sequence such as x-x-x-Y) (Chao et al., 2018; Gallimore et al., 2023; Xiong et al., 2024). Such local oddball responses depend on a simplified predictive model that the current stimulus will continue to repeat. However, local oddball responses persist during states of deep anesthesia when feedback connections are functionally weak (Nourski et al., 2018; Uhrig et al., 2016; Xiong et al., 2024). As such, they do not provide strong evidence for PC, which envisions rich and multi-faceted predictions feeding back and modulating early sensory processing (Kiebel et al., 2008; Wacongne et al., 2012). It is an open question whether sensory cortex is engaged by more complex prediction errors (Gabhart et al., 2023). More complex prediction error computations and higher-order predictions can be studied using “global oddballs”. These second-order pattern violations occur when a repeated presentation of first order pattern violations is interrupted (e.g., x-x-x-Y / x-x-x-Y / x-x-x-Y / x-x-x-X). Global oddballs are themselves a repeated stimulus, so responses cannot be explained by recent stimulus history, i.e., release from adaptation. There is evidence from human and non-human primate studies using functional Magnetic Resonance Imaging (fMRI), magneto- and electroencephography (M/EEG), and local field potential (LFP) for global oddball codes in sensory cortex (Gabhart et al., 2023).

However, two prior studies measuring spiking activity failed to find global oddball encoding in sensory cortex (areas V1 and V4 of macaques (Solomon et al., 2021) and mid-level auditory area Tpt (Xiong et al.,

2024)). In addition, two other studies reported neuronal signatures of global oddballs in higher-order prefrontal cortex (Bellet et al., 2024; Xiong et al., 2024), which were dependent on the conscious state (Xiong et al., 2024). Other studies in rodents find either positive (Bastos et al., 2023; Furutachi et al., 2024; Gallimore et al., 2023) or negative (Jamali et al., 2024) evidence for predictive coding computations that drive robust sensory representations as hypothesized. The apparent discrepancies between the above studies are complicated by the fact that each differed in the paradigm, species, as well as areas studied. As a consequence, the fundamental questions of if, when, and how hierarchical predictive coding emerges across the cortical hierarchy, or whether it is a ubiquitous phenomenon across mammals largely remain unanswered (Gabhart et al., 2023). To resolve this impasse, we tested core tenets of the hierarchical predictive coding model using Multi-Area, high-Density, Laminar-resolved Neurophysiological (MaDeLaNe) recordings of spiking activity in mice and monkeys that were habituated to form strong predictions about a stimulus sequence. Leveraging the unique capacity offered by combining the large-team based OpenScope Project with primate neurophysiology, we sampled across multiple stages of the visual cortical processing pathway, ranging from primary visual cortex to high-level visual and prefrontal areas. Using optogenetics in mice, we also tested whether specific inhibitory cell types (Parvalbumin- and Somatostatin-positive interneurons, the primary interneuron types that directly inhibit pyramidal neurons (Pfeffer et al., 2013)) were involved in oddball processing.

The unique combination of these techniques allowed us to test three core hypotheses postulated by hierarchical predictive coding (Figure 1A, Bastos et al., 2012; Friston, 2010; Rao and Ballard, 1999). We tested these hypotheses for both local and global oddballs. The first hypothesis (H1) tests the assumption that prediction error computations constitute a feedforward cortical mechanism. If so, then prediction errors should (a) be encoded early in the sensory response (within the first 50-150 ms of processing), (b) emerge early in the sensory cortical hierarchy and then subsequently in higher areas, (c) evoke activity in pyramidal neurons in superficial layers (L2/3) of cortex, as feedforward projections anatomically project from these neurons, and (d) evoke a feedforward pattern of directed functional connectivity between neurons. The second hypothesis (H2) is that if prediction error constitutes a core cortical computation, neuronal oddball processing should be robust and widespread (i.e., observed widely in different cortical areas and species). The third hypothesis (H3) is that if predictions are subtractive, they should involve the activation of inhibitory interneuron cell populations, and a release from their inhibition during prediction errors.

Consistent with the hypothesis of feedforward prediction error computations (H1), we found that local oddballs were first detected in primary visual cortex (V1) followed by higher areas, were primarily initiated by L2/3 neurons, and recruited a substantial neuronal population in each area. In contrast, global oddball sensory prediction error responses were absent in most visual areas, directly contradicting H2. Instead, they evoked a later, weaker, and sparser neuronal response. Superficial L2/3 did not preferentially encode global oddballs. We also tested the hypothesis that prediction errors feed forward by analyzing neuronal spiking time courses with Granger causality (Dhamala et al., 2008). We did not find a feedforward pattern of activation evoked by global oddballs, again contradicting H1, but did so for local oddballs, in line with (H1). Neither global nor local oddballs involved a release from predictive suppression mediated by PV+/SST+ inhibitory interneurons, thus failing to provide evidence for (H3). These results indicate that while local oddballs follow many of the principles proposed by predictive coding (H1, and H2, but not H3), global oddballs - which uniquely detect prediction violations that cannot be explained more simply by a release of adaptation - do not. These results challenge the core hypothesis that cortical neurons are ubiquitously engaged in complex predictive coding computations via a cortical microcircuit dedicated to computing prediction error, and suggest updates to PC are needed.

Results

To evaluate Predictive Coding (PC) hypotheses, we habituated both mice and macaques to a local oddball sequence for several days before recording neuronal responses to those local oddballs. We then introduced

2nd order global oddballs on the recording day (Figure 1B-E). We designed this extensive habituation procedure in order to ensure that animals had sufficient exposure to the local oddball sequence (e.g., x-x-x-Y) before the start of the experiments. On the recording day for mouse experiments, 6 Neuropixels probes were inserted into visual cortical areas (Figure 1F) where measurable visual responses were identified with expected response latencies as a function of area (Figure 1G). Measurable responses were present across each presentation in the sequence (Figure 1H). Crucially, the animals recognized the oddballs, as reflected by their pupillary response during both types of oddballs (Figure 1I).

Two cohorts of mice, each habituated to a different stimulus sequence, participated. To counterbalance the stimulus set across the population of animals, one cohort was habituated to a sequence of 3 rightward oriented gratings followed by a leftward oriented grating (x-x-x-Y, we refer to each stimulus in order as P1, P2, P3, P4), the other cohort to 3 leftward then a rightward (y-y-y-X). Following a 500 ms baseline, each stimulus was presented for 500 ms (with 500 ms interstimulus interval), for a total trial duration of 4500 ms (Figure 1E). Mice were habituated to these sequences (n=8 mice for x-x-x-Y and n=8 mice for y-y-y-X sequences) over the course of 5 sessions for a total of 2000 trials. Two macaques were habituated to these sequences with the additional requirement of central fixation of the eyes on the screen. Monkeys were habituated over the course of 3 sessions for a total of 2850 complete trials prior to recordings. Then, in the experimental session, mice/monkeys were exposed to the not-yet-experienced global oddball sequence with a lesser frequency (20%). After that experimental (global-local oddball, or “GLO”) block, mice/monkeys experienced a block of random orientation sequences (“Random” block) before the “Control” block where animals viewed repeated x-x-x-x sequences followed by a y-y-y-y sequences, rendering the same stimuli used in global oddball trials predictable. These controls were included for evaluating oddball detection in conjunction with the responses in the GLO experimental block.

The primary comparison of interest is composed of the response to the oddball stimulus during the GLO block (i.e., presentation 4 (P4) of either the local or global oddball sequences) and the response to the identical stimulus in the same sequence position of the Control block. To account for any non-specific differences between blocks, we normalized responses by subtracting the activity of the prior stimulus (presentation 3, P3). For global oddballs (x_1-x_2-x_3-X), this results in X - x_3 in the GLO block as compared to X - x_3 in the Control block. Global oddball status is defined by the prediction of the 4th stimulus in the block where X in the experimental block is unexpected and X in the control block is expected. For local oddballs (x_1-x_2-x_3-Y), this results in Y - x_3 in the GLO block as compared to Y - y_3 in the Control block where local oddball status is defined by the stimulus deviation (oddball), or lack thereof (control), of the 4th stimulus in the block relative to its prior stimuli. Significant oddball detection was determined via statistical comparison of the difference of differences for each oddball type (P4-P3 GLO block vs. P4-P3 control block) using a nonparametric, cluster-based permutation test to control for multiple comparisons (see Methods). We used this comparison at the population and single-unit level to evaluate the role of areas, layers, and cell types for oddball detection.

Local Oddballs

Based on recent work (Hamm and Yuste, 2016; Pak et al., 2021; Westerberg et al., 2021, 2023; Yan et al., 2018), we expected local oddballs to initially evoke enhanced spiking responses at the earliest stages of visual processing (H1, Figure 1A). We specifically hypothesized that local oddball detection occurs first in early visual cortical areas (i.e., V1) before being fed forward to later stage areas with a measurable delay.

We found that the local oddball evoked an increase in neuronal spiking throughout the visual hierarchy (Figure 3). This increased response cannot be explained by the fact that the oddball is a different stimulus (compared to the rest of the stimulus sequence) since we averaged across all neurons (thus eliminating any tuning-based preferences for one or the other stimulus), and about half of the animals saw the orthogonal orientation as the oddball stimulus. Moreover, across all recorded single-units in the dataset, we found a highly similar number of units strongly preferring each of the two orientations (LO-orientation: 21.2% of all single-units, GO-orientation: 22.3% of all single-units). This indicates that there was not a strong response bias

for one oddball feature over the other within the population of measured units. To summarize, even after completely randomizing neuronal biases, the local oddball stimulus consistently evoked a larger response when we examined spiking activity across layers, areas, and animals.

The grand average local oddball response (Figure 2C) featured another remarkable difference to all other responses - a profound oscillatory component with a cycle of ~5 Hz. While the magnitude of this oscillation diminished over the course of the 1s stimulus presentation, it remained present until stimulus offset, and could even be observed for another cycle or so after stimulus offset (Figure 1H).

Local oddball detection was present in the majority of single-units measured across brain areas (Figure 2A), supporting our second hypothesis (H2, Figure 1A). At the population level, local oddball detection was measured earlier in lower-order visual areas before emerging in higher-order visual areas (Figure 2B). This was concomitant with the median latency of visual onset responses of these areas, indicating feedforward propagation, as suggested by (H1) (see also directed functional connectivity analysis, Figure 4). However, when assessing cell types identified as critical for the neural instantiation of PC (Bastos et al., 2012) (Figure 1A, layer 2/3 pyramidal cells, inhibitory interneurons), we found that these populations show enhanced (without any reduction in the inhibitory interneurons, as would be implied by H3) activation to the local oddball compared to the control condition (Figure 2C, D). In the case of the layer 2/3 pyramidal cells of area V1 at the population level, we found greater local oddball detection within those units as compared to other V1 units, consistent with a feedforward propagation of the local oddball prediction error (H1). Altogether, we largely found support for the (H1 and H2) core predictions of the neural instantiation of PC in the local oddball responses (H3: inhibitory neuron activity was an exception).

Hierarchical Profiles of Global Oddballs do not reveal feedforward prediction error

Global oddball responses, which allow to rigorously test between PC and simpler alternative explanations such as stimulus history/adaptation, were markedly different. First, detection of global oddballs was restricted to only a few brain areas at the population level (areas LM, AM, and PM, Figure 3A). We also observed that higher-order brain areas detected the global oddball (AM: 336 ms post-stimulus, PM: 384 ms post-stimulus) earlier than the hierarchically earlier area (LM: 394 ms post-stimulus). At the individual unit level, only about 6% of all units showed significant global oddball detection across areas (Figure 3B) and there was little consistency when the detection emerged across units (examples in Figure 3C). Previous reports have suggested that sensory prediction errors signaling might be isolated to neuronal populations which are selective for the features that define the error producing stimulus (Furutachi et al., 2024). To test for this possibility, we isolated the population of GO-orientation selective neurons within our recorded populations and determined whether they specifically harbored a global oddball detection signal. Of the 22.3% of single-units that were strongly selective for the GO-orientation (relative to the LO-orientation), only 6.1% were also significant GO detectors. This is comparable to the rate of GO detectors we observed in the general population (6.4% of single-units). In other words, GO detection was not isolated to feature selective populations nor were all units highly selective for the GO stimulus found to be GO detectors.

Next, we evaluated laminar differences in global oddball detection. For this, we limited analysis to higher- (AM, PM) vs. lower-order (LM) cortex where we observed significant population global oddball detection. We divided the units into extragranular vs. granular compartments which should primarily reflect bottom-up vs. top-down driven factors contributing to global oddball detection. We observed significant population global oddball detection in only the extragranular compartments, and earlier in higher-order cortex (337 ms post-stimulus) than lower-order cortex (401 ms post-stimulus) (Figure 3D).

To address the directed propagation of oddball responses throughout the hierarchy, we next calculated Granger causality (GC, see Methods) to quantify directed functional connectivity amongst neurons. For each cortical area and mouse, we combined all available single neurons to create a population spiking time series (a minimum of N=12 neurons per area were used to create this population spiking time series). We then calculated GC between each pair of cortical areas, using the anatomical hierarchical ordering: V1, RL, LM, AL,

PM, AM (in order from earliest to latest area in the mouse visual hierarchy, Harris et al., 2019). This generated a total of 30 inter-areal GC values, one for each area pair and direction of influence. For each pair of areas, we computed the GC hierarchical asymmetry by subtracting feedforward GC minus feedback GC. For example, the feedforward GC from V1 to RL was subtracted from the feedback GC from RL to V1. A positive difference indicates that feedforward GC > feedback GC. A positive difference for both local and global oddballs would be consistent with the hypothesized (H1, Figure 1A) feedforward propagation of prediction error. We compared oddball GC responses during stimulus processing in both the early (100-300 ms post-oddball onset) and late (300-500 ms post-oddball onset) time windows between local and global oddballs and compared them to baseline (100 ms pre-oddball onset to 100 ms post-oddball onset). GC became significantly hierarchically asymmetric in the feedforward direction for local, but not global, oddballs during both early and late time periods (Figure 4B-D, Wilcoxon ranksum test of GC hierarchical asymmetry values across mice vs. pre-oddball baseline, $P<0.01$). In contrast, GC hierarchical asymmetry did not change during global oddballs compared to baseline (Figure 4B-D, Wilcoxon ranksum test of GC hierarchical asymmetry values across mice vs. pre-oddball baseline, all comparisons, $P>0.01$).

To determine whether top-down prediction signatures might be latent in synaptic dynamics rather than spiking activity, we examined the Current Source Density (CSD, a measure of local net depolarization) profiles during global oddball detection. CSD is frequently used as a proxy for synaptic activity occurring along the cortical column (Cox et al., 2019; Godlove et al., 2014; Kajikawa et al., 2017; Maier et al., 2010, 2011; Mehta et al., 2000a, 2000b; Ninomiya et al., 2015; Schroeder et al., 1998; Self et al., 2013; van Kerkoerle et al., 2014a, 2017; Westerberg et al., 2019, 2021, 2022, 2023) which reliably reflects columnar processing dynamics, including those that may be missed by spiking activity (Herrera et al., 2022; Tovar et al., 2023, 2020). We computed CSD from the LFP responses to the GLO and control sequences (Figure 5A) and then performed the same global oddball contrast as with the spiking data. We hypothesized (H1, Figure 1A) that a difference in current sinks in the upper or deep layers of cortex might manifest when the prediction is different (i.e., when the global oddball stimulus is predicted in the control vs. when it is not in the experimental block). In the global oddball condition, we did not observe reliable changes in synaptic activation at the earliest stage of visual cortical processing (i.e. in V1, Figure 5B), neither before nor after visual stimulation. Specifically, we did not observe significant, reliable synaptic changes in the extragranular compartments which would be indicative of top-down influences deploying a prediction to earlier areas. We made the same observation in downstream visual cortical areas (Figure 5C). This indicates the predictions are not being deployed widely through synaptic modulations nor in the spiking activity as shown earlier.

In summary, we did not find support for a global oddball detection mechanism across all visual cortical regions, nor that global oddball detection propagated to the earliest stages of sensory cortical processing (e.g., V1). Collectively, these findings do not support our second hypothesis (H2, Figure 1A). Instead, we found sparse global oddball detection, limited to higher cortical regions and in laminar compartments more often associated with cortical feedback than feedforward activity. Local oddballs, which can be explained by stimulus history alone, but not global oddballs, which are more indicative of genuine prediction violations, evoked feedforward connectivity amongst visual cortical neurons.

Global Oddballs: Lacking Expected Cell-type Involvement

While the observability of PC elements in global sensory prediction errors appears far more limited in scope than in the case of local oddballs, it is conceivable that the specific cell types critical to the neural instantiation of PC still play a critical role in global oddball detection in sensory cortex. Therefore, we next reevaluated global oddball detection with more careful consideration of the layer 2/3 pyramidal cells, which have been suggested to reflect the feedforward element of the prediction error, and the inhibitory interneurons, which have been hypothesized to show differential activation reflecting an instantiation of the subtractive prediction.

To identify layer 2/3 pyramidal units we eliminated single-units that were found to be inhibitory interneurons during the optotagging session for each animal, we eliminated units found outside layer 2 or 3,

and we ensured included units had spike waveform duration of longer than 0.4 ms (Figure 6A), which primarily reflects broad-spiking pyramidal cells (Foehring et al., 1991; González-Burgos et al., 2004; Henze et al., 2000; McCormick et al., 1985; Mitchell et al., 2007; Nowak et al., 2003; Povysheva et al., 2006; Tasker et al., 1996). At the population level, we found that putative layer 2/3 pyramidal cells did not signal global oddball detection (Figure 6B). In fact, we observed that an even smaller proportion of putative layer 2/3 pyramidal units (5% of single units) significantly detected global oddballs as compared to the unrestricted set of all units (6% of all single units) (Figure 6C, failing to support H1, Figure 1A). However, there were sparse units that signaled the global oddball in all measured areas except area AL (an example single unit response is shown in Figure 6D).

In PC, a subtractive element explains away expected input. This has been posited to be neuronally instantiated at the level of inhibitory interneuron populations (Bastos et al., 2012). Somatostatin- (SST) and Parvalbumin- (PV) expressing interneuron populations were identified with optotagging (Figure 7A, see Methods). PV+/SST+ units were identified across all brain areas of interest (Figure 7B) and on average showed discernable responses to the stimulus sequences (Figure 7C). However, we did not observe a substantial population of either interneuron type acting as global oddball detectors, although sparse individual examples could be observed (Figure 7D). The population averages showed no significant global oddball detection, indicating a minor role, if any role at all, for these populations in detecting global oddballs in sensory cortex (failing to support H3, Figure 1A).

Global Oddballs: Higher-order Detection Outside Sensory Cortex

To determine whether these results are consistent across species, we recorded an additional data set from a cohort of macaque monkeys (n=2). On the recording day for the monkey experiments, 1-4 high-density deep array probes (Diagnostic Biochips, see Methods) and/or V probes (Plexon) were inserted into the visual cortex and frontal cortex. The monkeys experienced identical patterns of oddball sequences (Figure 8A). They also showed significantly different pupillary responses to oddball presentations as determined using the same methods as the mice (Figure 8B), indicating they also recognized the oddballs as such. Electrode arrays were implanted in frontal cortical regions (FEF, PFC) as well as six visual cortical areas (V1, V2, V3, V4, MT, MST). Visual cortex recordings can be used to test whether predictive coding is a widespread, ubiquitous phenomenon across species (H2, Figure 1A).

The first and most apparent observation was that the pattern of local vs. global oddball detection is largely consistent between species. Local oddballs were detected across all measured brain areas in the monkey (Figure 8C, left). Similar to the mouse, global oddballs followed a roughly inverse hierarchical pattern. They emerged first in FEF (32 ms), next in V3/PFC (91/128 ms), then in MT (160 ms) (using the same statistical tests as in the mouse). Global oddball representation was not detected at the earliest stages of visual processing (V1 and V2). Also worth noting is that there was significant global oddball detection in both of the prefrontal areas and the associated modulation is stronger than that observed in sensory cortex. This, too, demonstrates the relatively sparse representation of global oddballs in sensory cortex and a pattern of spiking activity more indicative of feedback than feedforward processing (which fails to support H1 and H2, Figure 1A). In sum, our findings were largely consistent across species: we observed that global oddball detection is robustly signaled in prefrontal cortex even though its propagation through the visual cortex is relatively limited, weak, and late in the temporal evolution of the response.

Discussion

Local vs. Global Oddballs

In this study, we tested the neuronal implementation of predictive coding computations across visual and higher-order cortex in rodents and primates. We implemented an extensive habituation period that exposed

subjects to a predictable sequence (e.g., x-x-x-Y) for multiple sessions. This enabled subjects to create an internal predictive model. We aimed to test whether deviations from this model (prediction errors) were signaled when subjects were shown global oddballs (e.g., x-x-x-x) on 20% of trials on recording days. We performed an extensive survey of spiking responses throughout the visual cortex of mice and monkeys using MaDeLaNe (Multi-Area, high-Density, Laminar Neurophysiology) recordings (Gabhart et al., 2023), which we argue are necessary to inform neuronal tests of PC which invoke mechanisms at the level of cortical layers, areas, and distinct neuron types. We tested three core hypotheses of current PC models (Figure 1A, Bastos et al., 2012; Friston, 2005; Rao and Ballard, 1999) by examining coding of local and global oddballs. These models hypothesized prediction error computations to invoke feedforward mechanisms, be robust and widespread, and engage release from predictive suppression by modulating inhibitory interneuron activity.

Local oddballs largely followed this pattern. They emerged early in time, in superficial layers, and fed forward. The feedforward nature of local oddballs was evident both in temporal order of spiking response and as measured by directed functional connectivity analysis. Local oddballs engaged a robust and wide-spread response, recruiting around half the neurons in all visual cortical areas in both species. However, local oddballs did not result from a reduction in levels of PV+/SST+ inhibitory neuron activity - these inhibitory neurons also *increased* their firing rates during local oddballs. This implies that the predictive subtraction computation implied by predictive coding is not implemented via these inhibitory interneurons. Instead it seems more likely that local oddballs in this temporal context rely mostly on membrane-specific adaptation (Sanchez-Vives et al., 2000a, 2000b) and do not require feedback, as they survive (or are even enhanced) during anesthetized states (Nourski et al., 2018; Uhrig et al., 2016; Xiong et al., 2024). Therefore, local oddball responses by themselves do not provide strong evidence for ubiquitous PC (Gabhart et al., 2023), which envisions that prediction errors are the result of a subtraction between top-down prediction and bottom-up sensory drive under varying sensory and cognitive conditions.

In contrast to local oddballs, neuronal responses to global oddballs did not support PC hypotheses (Figure 1A). In sensory areas, global oddballs emerged late in the sensory response. Global oddballs emerged first in higher-order areas AM/PM in mice, and first in FEF in monkeys, and next in lower-order areas LM in mice and V3/MT in monkeys. This temporal progression resembled feedback processing more than it did feedforward. Global oddballs were not encoded in the population of putative pyramidal neurons in L2/3. Instead, they emerged weakly and sparsely in non-granular layers. This laminar pattern of neuronal response is more indicative of cortical feedback, not feedforward activation as hypothesized. Global oddballs should have elicited prediction error responses. But they were only detected in a small number of neurons in each area (3-9%). Inhibitory interneurons did not selectively encode the global oddballs.

Predictive Coding is not a ubiquitous feedforward process

Predictive coding (PC) models have hypothesized that a core cortical computation is prediction error (Bastos et al., 2012; Friston, 2005; Mumford, 1992; R. P. N. Rao and Ballard, 1999). We set up our task so that subjects were highly habituated to a particular sequence (e.g., x-x-x-Y) such that its violation (e.g., x-x-x-X) should drive robust neuronal representations of prediction error. In PC the habituated local oddballs (e.g., x-x-x-Y) should not drive much of a prediction error signal because they were fully predictable. To reiterate: under PC, neuronal encoding of the local oddball in our paradigm should be weak (as it is predictable, so should be subtracted away) and encoding of the global oddball should be robust (as it is a violation to a well-established pattern). We found the opposite. Spiking responses of cortical neurons robustly encoded unsurprising local oddballs but weakly encoded surprising global oddballs. Neither oddball type engaged a release of inhibition from PV/SST+ interneurons. Global oddballs, when they elicited responses, first engaged higher cortical areas typically associated with cognitive (e.g., PFC), not sensory functions (Miller and Cohen, 2001). This argues against the ubiquity of predictive coding signals in the cortex, especially in sensory cortex.

Another core tenant of predictive coding models is that prediction error computations were hypothesized to feed forward. This hypothesis describes local oddball processing relatively well. However, global oddball processing was better described by a feedback pattern of processing. Global oddballs emerged late in the sensory response and in higher-order areas first, then lower-order areas (in order of increasing hierarchical level for mice: 394 ms in LM, 384 ms in PM, 336 ms in AM, in order of increasing hierarchical level for macaques: 91 ms in V3, 160 ms in MT, 32 ms in FEF, 128 ms in PFC). Putative excitatory pyramidal neurons in L2/3 (which project feedforward connections) and their associated current sinks did not encode global oddballs. During local oddballs, Granger causality analysis showed a robust increase in feedforward directed functional connectivity, with lower-order areas (V1, LM, and RL) increasing their functional influence on higher areas (AL, AM, and PM). This enhanced feedforward connectivity was not observed during global oddballs. Therefore, by four independent metrics, including hierarchical area, temporal order, Granger causality and laminar compartment of spiking/current flow, we failed to detect feedforward processing during global oddballs. This violates a core tenet of PC models that hypothesized a substantial engagement of L2/3 pyramidal neurons in sensory cortex that transmit prediction errors in the feedforward direction.

Instead, our findings point to the engagement of cortical feedback as the predominant pathway by which global oddballs are signaled. This was seen in the temporal latencies of global oddball responses which first activated higher-order cortex as well as the laminar pattern of activation: global oddballs were found to emerge at the population level in the non-granular layers. These non-granular layers are more closely associated with feedback processing, not feedforward processing.

Caveats

While our findings demonstrate that the hypothesized ubiquitous elements of Predictive Coding are more nuanced, there are other crucial considerations that must be taken into account. For one, we have chosen to study pure global oddballs, which are deviations from expectations that are induced by the lack of a stimulus change. It is possible that other forms of expectation that do depend on local stimulus change (e.g., such as a local oddball which is also a global oddball) are encoded in sensory cortex (e.g., Furutachi et al., 2024; Jamali et al., 2024). However, more complex forms of prediction processing which were envisioned by PC models, such as the global oddball and omission responses (as in Kiebel et al., 2008; Wacongne et al., 2012), do not appear to robustly engage sensory cortical representations.

Another important consideration is the degree of attention that is paid to the oddballs by the animals. Previous work suggested that global oddballs cannot be observed under certain states of unconsciousness (Nourski et al., 2018; Xiong et al., 2024). Given the close relationship between conscious awareness and attention (Maier and Tsuchiya, 2021), it is possible that attention serves as a prerequisite for global oddball processing (Bekinschtein et al., 2009). Given the pupillary responses of the animals in these experiments (Figure 1I, 8B), it is likely that the animals recognized the oddball stimuli (both local and global) as oddballs. Also, the finding that local oddballs evoked reliable activity in ~50% of neurons suggests that sufficient attention was present to the stimulus sequences. Finally, global oddballs were observed in prefrontal areas in monkeys and in higher-visual areas in mice, and thus despite being available to the animals' higher-cortex and evident in behavior as measured by pupil responses, did not have a profound effect on sensory responses.

Also, hierarchical predictive coding models have postulated that prediction error signals are modulated by a gain term that takes on a functional interpretation in terms of precision (Π in Figure 1A, see also (Feldman and Friston, 2010)). That being said, models that consider gain in terms of precision require that precision must be positive and nonzero (Bolstad and Curran, 2016), entailing that prediction error signals might be attenuated, but are never entirely quashed, by gain modulation. Future studies should explicitly consider the role of gain modulation on prediction error responses by manipulating the attentional state.

Updates to Predictive Coding models

Our results challenge core hypotheses of current PC models (Figure 1A). Global oddballs emerged in hierarchically late areas in both species. They did not feedforward throughout the visual cortex and did not preferentially engage feedforward projecting layers 2/3. Local oddballs, given their extensive habituation, should have been an unsurprising stimulus evoking minimal prediction error. Yet, they engaged activity in over half of recorded cortical neurons. Global oddballs were designed to be a surprising stimulus to evoke strong prediction errors. But they did not engage a robust response in visual cortex, neither in mice nor in monkeys. Instead, global oddballs were initially signaled late in hierarchical processing, area AM in mice, prefrontal area FEF in monkeys. So although global oddballs are available at high levels of the hierarchy and could in principle have informed and guided sensory processing, they did not drive a prediction error response in sensory cortex as hypothesized by PC.

While our results rule out most PC models from the existing modeling literature, the broader family of predictive processing theories have resources for new models that could capture the effects we observe. The most prominent such resource involves the brain representing a hierarchy of time-scales (Kiebel et al., 2008) ranging from the very short in primary sensory cortex to the more long-term in higher-order areas such as PFC; the models given detected a stimulus omission only with the longer-term, higher-order generative model. Such a theory would imply that we only observe prediction-error encoding in regions of the brain representing the stimulus or task at a sufficiently long timescale to capture the prediction error induced by the oddball stimulus. Generative models based on Slow Feature Analysis have previously captured observed properties of a number of sensory and higher-order cell types (Berkes and Wiskott, 2005; Dähne et al., 2014; Franzius et al., 2007); PC could serve as a learning mechanism for such models.

Rather than being a computation that originates at the level of sensory processing, these data thus lead us to propose that prediction errors are computed in higher-order areas such as PFC. Higher areas such as the PFC display the property of mixed selectivity (Rigotti et al., 2013). Neurons in these areas have response properties that are not based on sensory bottom-up features and are more flexible with regard to response preferences. These higher-order neurons can re-map their activity in real-time based on experience-dependent learning. This property is ideal for representing predictions, which map out the statistical structure of a changing and context-dependent environment. Therefore, the neuronal instantiation of prediction itself requires a flexible, dynamic mechanism to adapt to changing environments. Neurons in sensory cortex, with receptive field properties defined at evolutionary time scales and further refined during development, seem ill-suited for such a computation.

We propose instead that ensembles of PFC neurons (and neurons in other higher-order areas) generate predictions based on experience-dependent learning. This ensemble learning may be facilitated by beta-rhythmic oscillations that have properties seemingly ideal for formation of predictions. Namely, they can form neuronal ensembles in a dynamic and cognition-dependent manner (Antzoulatos and Miller, 2016; Buschman et al., 2012; Miller et al., 2018) and are associated with feedback communication in cortex (Bastos et al., 2015; Michalareas et al., 2016; van Kerkoerle et al., 2014b; Vezoli et al., 2021). This pattern of predictive activity (as well as violations to prediction) can then be communicated selectively and sparsely via top-down feedback to sensory cortex. This notion is consistent with global oddballs evoking a feedback pattern of activity. It is also consistent with our observation of sparse and less wide-spread patterns of global oddball responses and the absence of predictive information in primary and secondary sensory areas. In contrast, unsurprising local oddballs were robustly encoded in cortex and drove strong feedforward processing. To summarize, based on the global oddball paradigm and an extensive spiking survey of cortical activity in mice and monkeys, our data indicate that sensory feedforward processing is not primarily engaged in prediction error computations as traditional PC models hypothesized.

Predictive codes are not a ubiquitous property of cortical processing that drive sensory cortical responses. Instead, they are largely a property of higher-order neurons, conveyed to sensory areas in a selective and sparse manner, and with a modulatory nature.

Methods

Animals

Mouse Experiments at the Allen Institute

All experiments were performed in 16 SSTAi32 and PVAi32 mice (*mus musculus*) of both sexes (n_{male}=6, n_{female}=10), aged 95-128 days. Optogenetics experiments were conducted with Sst-IRES-Cre/wt; Ai32(RCL-ChR2(H134R)_EYFP)/wt mice (n=9) and Pvalb-IRES-Cre/wt; Ai32(RCL-ChR2(H134R)_EYFP)/wt) mice (n=7). Pvalb-IRES-Cre and Sst-IRES-Cre mice were bred in-house and crossed with an Ai32 channelrhodopsin reporter line. Pvalb-IRES-Cre;Ai32 breeding sets (pairs and trios) consisted of heterozygous Pvalb-IRES-Cre mice crossed with either heterozygous or homozygous Ai32(RCL-ChR2(H134R)_EYFP) mice. Pvalb-IRES-Cre is expressed in the male germline. To avoid germline deletion of the stop codon in the loxP-STOP-loxP cassette, Pvalb-IRES-Cre;Ai32 mice were not used as breeders. Sst-IRES-Cre;Ai32 breeding sets (pairs and trios) consisted of heterozygous Sst-IRES-Cre mice crossed with either heterozygous or homozygous Ai32(RCL-ChR2(H134R)_EYFP) mice. Cre+ cells from Ai32 lines are highly photosensitive, owing to the expression of Channelrhodopsin-2. All experiments on animals were conducted with approval of the Allen Institute's Institutional Animal Care and Use Committee.

Macaque Monkey Experiments at Vanderbilt University

All procedures were approved by the Vanderbilt University Institutional Animal Care and Use Committee, in compliance with the regulations set by the Association for the Assessment and Accreditation of Laboratory Animal Care, and followed the guidelines of the United States National Institutes of Health. Two macaque monkeys were used in this study: one male adult bonnet macaque (*Macaca radiata*) aged 19 years (Ca, 7.4kg), and one male adult rhesus macaque (*Macaca mulatta*) aged 11 years (Jo, 12.0 kg).

Surgery

Mouse Experiments at the Allen Institute

The surgery pipeline at the Allen Institute is described in detail in previous reports (Durand et al., 2023; Siegle et al., 2021). Briefly, A pre-operative injection of dexamethasone (3.2 mg kg^{-1}, subcutaneously (s.c.)) was administered 1 h before surgery to reduce swelling and postoperative pain by decreasing inflammation. Mice were initially anesthetized with 5% isoflurane (1–3 min) and placed in a stereotaxic frame (Model 1900, Kopf). Isoflurane levels were maintained at 1.5–2.5% for the duration of the surgery. Body temperature was maintained at 37.5 °C. Carprofen was administered for pain management (5–10 mg kg−1, s.c.) and atropine was administered to suppress bronchial secretions and regulate hearth rhythm (0.02–0.05 mg mg kg−1, s.c.). An incision was made to remove skin, and the exposed skull was levelled with respect to pitch (bregma–lambda level), roll and yaw. The headframe was placed on the skull and fixed in place with White C&B Metabond(Parkell). Once the Metabond was dry, the mouse was placed in a custom clamp to position the skull at a rotated angle of 20°, to facilitate creation of the craniotomy over the visual cortex. A circular piece of skull 5 mm in diameter was removed, and a durotomy was performed. The brain was covered by a 5-mm-diameter circular glass coverslip, with a 1-mm lip extending over the intact skull. The bottom of the coverslip was coated with a layer of polydimethylsiloxane (SYLGARD 184, Sigma-Aldrich) to reduce adhesion to the brain surface. The coverslip was secured to the skull with Vetbond (Patterson Veterinary). Kwik-Cast (World Precision Instruments) was added around the coverslip to further seal the implant, and Metabond bridges between the coverslip and the headframe well were created to hold the Kwik-Cast in place. At the end

of the procedure, but before recovery from anesthesia, the mouse was transferred to a photodocumentation station to capture a spatially registered image of the cranial window.

Intrinsic signal imaging was performed to identify visual area boundaries (Juavinett et al., 2017). Based on the identified visual areas, an insertion window was designed for each mouse. Mice were habituated to head-fixation and visual stimulation over a period of two weeks.

Macaque monkey experiments at Vanderbilt University

Monkeys were implanted with a head post and recording chambers during an anesthetized procedure. Monkeys were anesthetized with isoflurane. Body temperature was maintained near 38°C with a circulating water or warm air recirculating heating blanket. Peripheral oxygen levels as well as heart rate, temperature, ECG and expired CO2 levels were monitored continuously during surgery. The animals' head was shaved and scrubbed (with Betadine and ethanol) after mounting the animal in a stereotaxic device. Local anesthetic (Lidocaine) was injected subcutaneously before opening and also placed into ear canals before fitting the animal into the stereotaxic device.

A skin flap was made over the skull. The skull was cleaned and dried, and orthopedic screws were placed in the skull. The head restraint device, held in position with a stereotaxic holder, was fixed in place with orthopedic screws and methyl methacrylate cement. Custom-made recording chambers (~20 mm in diameter, Crist Instruments) were placed on the skull to allow access to all targeted brain areas in one hemisphere and secured in place with orthopedic screws and dental cement. Craniotomies (10-20 mm diameter) were subsequently performed using piezosurgery drills (Piezosurgery, Columbus, Ohio) to permit access to the underlying cortex. Monkey Ca had two recording chambers, one placed over the prefrontal cortex (giving access to areas FEF and LPFC) and one placed over the temporal cortex (giving access to areas MT, MST, V4, and TEO). Monkey Ca had one recording chamber positioned over the occipital cortex (giving access to areas V1, V2, V3). After surgery, analgesics were given for pain management (Buprenorphine and NSAIDs for 3 days), and animals showed no signs of pain or distress.

Electrophysiology Experiments

Mouse Experiments at the Allen Institute

The Neuropixels data was acquired at the Allen Institute as part of the OpenScope project that allows the community to apply for observation on the Allen Brain Observatory platform (https://alleninstitute.org/division/mindscope/openscope/). The Neuropixels pipeline at the Allen Institute is described in detail in previous reports (Durand et al., 2023; Siegle et al., 2021).

On the day of recording, the cranial coverslip was removed and replaced with the insertion window containing holes aligned to six cortical visual areas. Mice were allowed to recover for 1–2 hours after insertion window placement, before being head-fixed in the recording rig.

Six Neuropixels probes were targeted to each of the six visual cortical areas (V1, LM, RL, AL, PM, AM). The boundaries of these areas and their retinotopic maps were obtained through intrinsic signal imaging, and insertion locations were planned to target regions responsive to the center of the LCD monitor. Probes were doused with CM-DiI (1 mM in ethanol; Thermo Fisher, V22888) for post hoc ex vivo probe localization. Each probe was mounted on a 3-axis micromanipulator (New Scale Technologies). The tip of each probe was aligned to its associated opening in the insertion window using a coordinate transformation obtained via a previous calibration procedure. XYZ manipulator coordinates were obtained via a previous calibration procedure where the tips of probes were aligned to the retinotopic centers of target visual areas using an image provided by intrinsic signal imaging. The operator then moved each probe into place with a joystick, with the probes fully retracted along the insertion axis, approximately 2.5 mm above the brain surface. The probes

were then manually lowered one by one to the brain surface until spikes were visible on the electrodes closest to the tip. After the probes penetrated the brain to a depth of around 100 μm, they were inserted automatically at a rate of 200 μm/min (total of 3.5 mm or less in the brain). After the probes reached their targets, they were allowed to settle for 5–10 min.

Neuropixels data was acquired at 30 kHz (spike band, 500 Hz high-pass filter) and 2.5 kHz (LFP band, 1,000 Hz low-pass filter) using the Open Ephys GUI (Siegle et al., 2017). Videos of the eye and body were acquired at 60 Hz. Pupil size was measured via previously described means (Siegle et al., 2021). Briefly, a universal eye tracking model trained in DeepLabCut (Mathis et al., 2018), a ResNET-50 based network, to recognize up to 12 tracking points each around the perimeter of the eye, the pupil, and the corneal reflection. The angular velocity of the running wheel was recorded at the time of each stimulus frame, at approximately 60 Hz.

The spike-band data was median-subtracted, first within-channel to center the signal around zero, then across channels to remove common-mode noise. The median-subtracted data file was sent through the Kilosort2 MATLAB package (https://github.com/mouseland/Kilosort2) (Pachitariu et al., 2023), which applies a 150 Hz high-pass filter, followed by whitening in blocks of 32 channels. Kilosort2 models this filtered, whitened data as a sum of spike 'templates'. The shape and locations of each template was iteratively refined until the data can be accurately reconstructed from a set of N templates at M spike times. Finally, Kilosort2 output was curated to remove putative double-counted spikes and units with artefactual waveforms. All units not classified as noise were packaged into Neurodata Without Borders (NWB) files (Rübel et al., 2022) and analyzed in this paper.

PV and SOM cells were identified in their respective mouse lines through a brief opto-tagging session (Lima et al., 2009). At the end of the neurophysiology session in each animal, cells were stimulated with an optical fiber at 40 Hz, 5 Hz, and with a raised cosine function in 1 s epochs. Cells whose mean response during the stimulation epoch which positively exceeded 2 standard deviations of their baseline, prestimulus (100 ms epoch) activity to any of the stimulation profiles were deemed as belonging to the associated interneuron group.

Current source density (CSD) (Freeman and Nicholson, 1975; Mitzdorf, 1985; Nicholson and Freeman, 1975; Nicholson and Llinas, 1971) was estimated from the LFP band data by epoching the LFPs, median-filtering with a filter-width of 3 channels, and then downsampling to every 4th channel to retrieve a single vertical/laminar column of responses. CSD was then estimated as the 2nd spatial derivative across multiple contact points according to the equation of (Mitzdorf and Singer, 1978):

$$CSD(t, c) = -\sigma\,(V(t, c-2) - 2V(t, c) + V(t, c+2))/(2s\text{^}2)$$

where *V(t, c)* is the extracellular voltage at time *t* measured at an electrode contact at position *c*, *s* is the inter-contact distance of the electrode array, and σ is the tissue conductivity (here taken as 0.4 S/m). CSD contrasts were computed by grand-averaging the raw LFPs over each condition, then calculating the CSD as above and subtracting across conditions. We corrected for time in task as a confounder via double contrasts**,** first subtracting the 3rd (fully adapted) presentation response from that of the 4th, and then pooling trials, within task conditions. These subtractions were treated as normal random variates for a two-tailed, nonparametric spatiotemporal cluster-test that controls the family-wise error rate to $p < 0.05$ to determine significant cross-condition contrasts (Maris and Oostenveld, 2007). Both LFP and CSD are smoothed with a width 4 Gaussian filter in both the spatial (laminar) and temporal dimensions for plotting.

Macaque Monkey Experiments at Vanderbilt University

We acquired data using between 1-4 linear array multi-channel recording probes. In most experiments, we recorded with 128-channel "deep array" probes where the inter-contact spacing was either 25 or 40 μm (Diagnostic Biochips, Glen Burnie, MD) and the coverage was 3.175 mm and 5.08 mm, respectively. In some

experiments, we used 32-channel V probes with an inter-contact spacing of 100 μm (Plexon, Dallas, TX) with a coverage of 3.1 mm. To insert electrodes into the appropriate depth and area we used a mechanical Microdrive (Narishige, Tokyo, Japan) that was mounted onto the chambers. A guide tube was lowered through a recording grid (Crist Instrument Co., Inc.) to penetrate the dura mater and granulation tissue. We then acutely introduced the recording probe into the respective area, and waited ~1 hour for the signal to settle prior to starting the recordings. Recordings were acquired using a RHD System (Intan, Los Angeles, CA) sampling at 30 kHz. Recordings were referenced to the guide tube which remained in contact with tissue. Grid positions were pre-determined based on a pre-recording MRI scan with the recording chambers and grid in place, with water to mark the trajectories of each grid hole position. We advanced the electrode until there was visually responsive neuronal activity on most channels and until the local field potentials showed a distinct spectral signature of the cortical sheet, characterized by large amplitude alpha/beta (10-30 Hz) oscillations in deep channels and gamma (40-150 Hz) oscillations in superficial channels (Maier et al., 2010; Mendoza-Halliday et al., 2024; Tovar et al., 2023, 2020; Westerberg et al., 2019). Offline, using MATLAB the data was filtered between 500-5000 Hz, full-wave rectified, low-pass filtered below 250 Hz, and downsampled to 1000 Hz. We refer to this signal as the MUAe signal and it reflects the activity of nearby surrounding neurons (Logothetis et al., 2001; Self et al., 2013; Supèr and Roelfsema, 2005; Tovar et al., 2020; Trautmann et al., 2019; Westerberg et al., 2023, 2020).

Visual Stimulation Parameters

Mouse Experiments at the Allen Institute

All Neuropixels recordings were according to the standardized Neuropixels visual coding pipeline. Visual stimuli were generated using custom scripts based on PsychoPy and were displayed using an ASUS PA248Q LCD monitor, with 1920 X 1200 pixels (55.7 cm wide, 60 Hz refresh rate). Stimuli were presented monocularly, and the monitor was positioned 15 cm from the right eye of the mouse and spanned 120 dva × 95 dva. Monitor placement was standardized across rigs such that mouse right eye gaze would typically be directed at the center of the monitor.

Macaque Monkey Experiments at Vanderbilt University

We used MonkeyLogic (developed and maintained at the National Institute for Mental Health) to control the behavioral task (Hwang et al., 2019). Visual stimuli were displayed using PROPixx Pro projectors (VPixx Technologies, Quebec, Canada) with a resolution of 1920 x 1080 at a 120 Hz refresh rate. The projector screen was positioned 57 cm in front of the monkey's eyes.

The monkey was trained to fixate its eyes around a central fixation dot (radius of fixation window: 1.5 dva). Eye position and pupil diameter was monitored using an Eyelink 1000 (SR Research, Ottawa, Canada) at either 250 or 500 Hz. A task began with an isoluminant gray screen. Once the monkey maintained fixation for 500ms, a sequence of drifting gratings appeared (12 dva radius, 2 Hz drift rate, 1 cycle/degree, 0.8 Michelson contrast, angle of drifting grating was 45 or 135 degrees from the vertical midline) for 500 ms, and was replaced by a blank screen with the fixation dot remaining for 500 ms. This sequence was repeated 4 times in a trial, for a total trial length of 4500 ms (500 ms pre-sequence fixation + 4x1000 ms stimulus presentations). The monkey was rewarded for maintaining fixation throughout the trial with a small juice reward.

Habituation to predicted sequence

Mouse Experiments at the Allen Institute

Mice were habituated over the course of 5 behavior-only sessions in which only the predicted sequence (either xxxY or yyyX) was presented. This resulted in 2000 habituation trials prior to recordings.

Macaque Monkey Experiments at Vanderbilt University

Monkeys were habituated to a predicted sequence over the course of 3 behavior-only sessions in which only the predicted sequence (either xxxY or yyyX) was presented. This resulted in 2850 complete habituation trials prior to recording sessions. Subsequently after a recording session, monkeys were again re-habituated to one of the predicted sequences prior to the next recording session.

Data Analysis

Mouse Experiments at the Allen Institute

We recorded 29977 total putative single-units, with an average of 359 (+/-42) units per animal and an average of 60 (+/-3) units per probe. We further restricted the units for analysis, consistent with previous reports using the same methods for analyses (Siegle et al., 2021), to those which exhibit a visual response that exceeded 5 standard deviations of the baseline firing rate, minimum of 0.1 sp/s, inter-spike interval (ISI) violations below 0.33, a presence ratio above 0.95, an amplitude cutoff below 0.1, and were found to be in areas V1, LM, RL, AL, PM, AM, or LP. This resulted in a sample of 5389 units from 15 of 16 mice. No units from 1 mouse passed criteria due to a destabilizing event during the recording. Additionally, data from another mouse were omitted from analysis due to issues with the visual stimulus timing. As a result, our final sample consisted of 5062 single-units from 14 mice.

Macaque Monkey Experiments at Vanderbilt University

We recorded a total of 6,619 sites with MUAe signals across 8 cortical areas across 19 recording sessions: 640 in PFC, 416 in FEF, 512 in MST, 512 in MT, 1056 in V4, 1536 in V3, 896 in V2, and 1024 in V1. These MUAe signals were extracted from broadband signal with a butterworth filter of stopbands at 450Hz and 5500Hz, and passbands at 500Hz and 5000Hz. For analysis, we restricted these sites that had visually evoked activity, which was determined by whether the time period from 50-250 ms post-stimulus was significantly greater than pre-stimulus baseline (using a threshold of $p<0.05$, rank sum test). This resulting population that was used for analysis consisted of 508 sites in PFC, 177 in FEF, 161 in MST, 252 in MT, 230 in V4, 569 in V3, 328 in V2, and 270 in V1.

Granger causality analysis

In mice, we began by defining all available single units in each area. We took all cortical neurons for this analysis, and per mouse and probe, included an area in the analysis if a minimum of 12 single neurons were simultaneously acquired. This resulted in a total of six neuronal spiking time series, one per area. Granger causality was calculated separately per mouse and separately for local and global oddball trials, using all available trials for the calculation. We calculated Granger causality using a non-parametric implementation (Dhamala et al., 2008; Nedungadi et al., 2009). For this, we computed fourier coefficients using the Fieldtrip toolbox (Oostenveld et al., 2011) using a sliding window approach utilizing 200 ms time windows for analysis. We computed the Fourier coefficients using multitapers (3 multitapers per trial, time window size = 200 ms, smoothing = 10 Hz, function ‘ft_freqanalysis’, using method ‘mtmfft’, frequencies 0-100 Hz were calculated). One time window was on the baseline, from 100 ms pre-oddball onset to 100 ms post-oddball onset. Two time windows reflecting stimulus processing were also used, one centered from 100 ms to 300 ms post-oddball onset, another from 300 ms to 500 ms post-oddball onset. Bivariate Granger causality was computed pair-wise between all available neuronal spiking time series (using ft_connectivity analysis with method = ‘granger’ and granger.sfmethod = ‘bivariate’).

Statistics and Visualization

All data was normalized by its average level of activity to produce an arbitrary value that was less variable across units with differing firing rates. Unless otherwise noted, all statistics were performed using nonparametric, cluster-based permutation testing (Maris and Oostenveld, 2007) of the spiking activity at either the single-(multi)unit level or at the population level with alpha thresholds set to 0.05 for both stages of the test. We additionally required that a statistically significant difference as indicated by this test persist for at least 25 ms. Data was smoothed with a 50 ms moving mean window. Confidence clouds, where displayed, are computed for a 95% confidence interval across units' condition-wise mean activity included in the population.

Feature selectivity was measured in the same way as a previous report (Furutachi et al., 2024). First, we determined the mean response to each of the stimuli during visual stimulation (0-500 ms following stimulus appearance) and during a separate presentation block where stimulus order was randomized. For each single-unit, we subtracted the mean response to GO-orientation stimulus from the LO-orientation stimulus and divided by the sum of those two means. Single-units with this index above 0.8 or below -0.8 were defined as highly selective for the GO-orientation or the LO-orientation, respectively.

Data and Code Availability

All mouse data used in this work are openly available through the DANDI Archive (dandiset id: 000253, doi: https://doi.org/10.48324/dandi.000253/0.240503.0152). Software resources for the analysis of this dataset are provided here: https://alleninstitute.github.io/openscope_databook/projects/glo.html. The code to generate the global-local oddball sequences is provided here: https://github.com/AllenInstitute/openscope-glo-stim.

Acknowledgements

This work was funded by the National Institutes of Health [grant number: R00MH116100] (A.M.B.), through Vanderbilt University Startup Funds (A.M.B.), and via funding from the Vanderbilt Brain Institute Faculty Fellow award (A.M.B.). J.A.W. was funded by a fellowship from the International Human Frontier Science Program Organization [grant number: LT0001/2023-L]. The Neuropixels dataset was obtained at the Allen Brain Observatory as part of the OpenScope program, which is operated by the Allen Institute, Neural Dynamics. OpenScope was supported by the National Institutes of Health [grant number: U24NS113646]. We thank Christof Koch and all members of the OpenScope steering committee for their support. We also thank the Allen Institute founder, Paul G. Allen, for his vision, encouragement, and support.

Declaration of Interests

The authors declare no competing interests.

Author contributions

Conceptualization: J.A.W., A.M., A.M.B.; Data curation: J.A.W., A.B., S.D., B.H., J.A.L.; Formal analysis: J.A.W., Y.S.X., E.S., A.M.B; Funding acquisition: J.A.W., J.A.L., A.M.B.; Performed data recordings in macaques: J.A.W., Y.X., H.N., A.M.B, Performed data recordings in mice: S.D., B.H., H.C., H.B., H.L, W.H., K.N., V.H., T.J., C.G., A.Y., J.S., R.G., B.O., S.D., S.C., A.W., P.A.G.; Project administration: J.A.W., C.K., J.A.L., A.M., A.M.B.; Software: J.A.W., A.B., C.R.P.; Supervision: S.R.O., J.A.L., A.M., A.M.B.; Validation: J.A.W., A.B., C.R.P., J.A.L.; Visualization: J.A.W., Y.S.X.; Writing - original draft: J.A.W., A.M., A.M.B.; Writing - review and editing: all authors.

References

Antzoulatos, E.G., Miller, E.K., 2016. Synchronous beta rhythms of frontoparietal networks support only behaviorally relevant representations. eLife 5, e17822. https://doi.org/10.7554/eLife.17822

Bastos, A.M., Usrey, W.M., Adams, R.A., Mangun, G.R., Fries, P., Friston, K.J., 2012. Canonical Microcircuits for Predictive Coding. Neuron 76, 695–711. https://doi.org/10.1016/j.neuron.2012.10.038

Bastos, A.M., Vezoli, J., Bosman, C.A., Schoffelen, J.-M., Oostenveld, R., Dowdall, J.R., De Weerd, P., Kennedy, H., Fries, P., 2015. Visual areas exert feedforward and feedback influences through distinct frequency channels. Neuron 85, 390–401. https://doi.org/10.1016/j.neuron.2014.12.018

Bastos, G., Holmes, J.T., Ross, J.M., Rader, A.M., Gallimore, C.G., Wargo, J.A., Peterka, D.S., Hamm, J.P., 2023. Top-down input modulates visual context processing through an interneuron-specific circuit. Cell Rep. 42, 113133. https://doi.org/10.1016/j.celrep.2023.113133

Bekinschtein, T.A., Dehaene, S., Rohaut, B., Tadel, F., Cohen, L., Naccache, L., 2009. Neural signature of the conscious processing of auditory regularities. Proc. Natl. Acad. Sci. 106, 1672–1677. https://doi.org/10.1073/pnas.0809667106

Bellet, M.E., Gay, M., Bellet, J., Jarraya, B., Dehaene, S., Kerkoerle, T. van, Panagiotaropoulos, T.I., 2024. Spontaneously emerging internal models of visual sequences combine abstract and event-specific information in the prefrontal cortex. Cell Rep. 43. https://doi.org/10.1016/j.celrep.2024.113952

Berkes, P., Wiskott, L., 2005. Slow feature analysis yields a rich repertoire of complex cell properties. J. Vis. 5, 9. https://doi.org/10.1167/5.6.9

Bolstad, W.M., Curran, J.M., 2016. Introduction to Bayesian Statistics, 3rd ed. Wiley. https://doi.org/10.1002/9781118593165

Brown, H.R., Friston, K.J., 2013. The functional anatomy of attention: a DCM study. Front. Hum. Neurosci. 7, 784. https://doi.org/10.3389/fnhum.2013.00784

Buschman, T.J., Denovellis, E.L., Diogo, C., Bullock, D., Miller, E.K., 2012. Synchronous oscillatory neural ensembles for rules in the prefrontal cortex. Neuron 76, 838–846. https://doi.org/10.1016/j.neuron.2012.09.029

Chao, Z.C., Takaura, K., Wang, L., Fujii, N., Dehaene, S., 2018. Large-Scale Cortical Networks for Hierarchical Prediction and Prediction Error in the Primate Brain. Neuron 100, 1252-1266.e3. https://doi.org/10.1016/j.neuron.2018.10.004

Cox, M.A., Dougherty, K., Westerberg, J.A., Schall, M.S., Maier, A., 2019. Temporal dynamics of binocular integration in primary visual cortex. J. Vis. 19, 13. https://doi.org/10.1167/19.12.13

Dähne, S., Wilbert, N., Wiskott, L., 2014. Slow Feature Analysis on Retinal Waves Leads to V1 Complex Cells. PLOS Comput. Biol. 10, e1003564. https://doi.org/10.1371/journal.pcbi.1003564

Dhamala, M., Rangarajan, G., Ding, M., 2008. Estimating Granger Causality from Fourier and Wavelet Transforms of Time Series Data. Phys. Rev. Lett. 100, 018701. https://doi.org/10.1103/PhysRevLett.100.018701

Durand, S., Heller, G.R., Ramirez, T.K., Luviano, J.A., Williford, A., Sullivan, D.T., Cahoon, A.J., Farrell, C., Groblewski, P.A., Bennett, C., Siegle, J.H., Olsen, S.R., 2023. Acute head-fixed recordings in awake mice with multiple Neuropixels probes. Nat. Protoc. 18, 424–457. https://doi.org/10.1038/s41596-022-00768-6

Feldman, H., Friston, K., 2010. Attention, Uncertainty, and Free-Energy. Front. Hum. Neurosci. 4. https://doi.org/10.3389/fnhum.2010.00215

Foehring, R.C., Lorenzon, N.M., Herron, P., Wilson, C.J., 1991. Correlation of physiologically and morphologically identified neuronal types in human association cortex in vitro. J. Neurophysiol. 66, 1825–1837. https://doi.org/10.1152/jn.1991.66.6.1825

Franzius, M., Sprekeler, H., Wiskott, L., 2007. Slowness and Sparseness Lead to Place, Head-Direction, and Spatial-View Cells. PLOS Comput. Biol. 3, e166. https://doi.org/10.1371/journal.pcbi.0030166

Freeman, J.A., Nicholson, C., 1975. Experimental optimization of current source-density technique for anuran cerebellum. J. Neurophysiol. 38, 369–382. https://doi.org/10.1152/jn.1975.38.2.369

Friston, K., 2010. The free-energy principle: a unified brain theory? Nat. Rev. Neurosci. 11, 127–138. https://doi.org/10.1038/nrn2787

Friston, K., 2005. A theory of cortical responses. Philos. Trans. R. Soc. B Biol. Sci. 360, 815–836. https://doi.org/10.1098/rstb.2005.1622

Friston, K.J., Parr, T., de Vries, B., 2017. The graphical brain: belief propagation and active inference. Netw.

Neurosci. 1–78. https://doi.org/10.1162/NETN_a_00018
Furutachi, S., Franklin, A.D., Aldea, A.M., Mrsic-Flogel, T.D., Hofer, S.B., 2024. Cooperative thalamocortical circuit mechanism for sensory prediction errors. Nature 633, 398–406. https://doi.org/10.1038/s41586-024-07851-w
Gabhart, K., Xiong, Y., Bastos, A., 2023. Predictive Coding: A more cognitive process than we thought? https://doi.org/10.31234/osf.io/7sz3w
Gallimore, C.G., Ricci, D.A., Hamm, J.P., 2023. Spatiotemporal dynamics across visual cortical laminae support a predictive coding framework for interpreting mismatch responses. Cereb. Cortex 33, 9417–9428. https://doi.org/10.1093/cercor/bhad215
Garrido, M.I., Kilner, J.M., Kiebel, S.J., Friston, K.J., 2007. Evoked brain responses are generated by feedback loops. Proc. Natl. Acad. Sci. U. S. A. 104, 20961–20966. https://doi.org/10.1073/pnas.0706274105
Godlove, D.C., Maier, A., Woodman, G.F., Schall, J.D., 2014. Microcircuitry of Agranular Frontal Cortex: Testing the Generality of the Canonical Cortical Microcircuit. J. Neurosci. 34, 5355–5369. https://doi.org/10.1523/JNEUROSCI.5127-13.2014
González-Burgos, G., Krimer, L.S., Urban, N.N., Barrionuevo, G., Lewis, D.A., 2004. Synaptic Efficacy during Repetitive Activation of Excitatory Inputs in Primate Dorsolateral Prefrontal Cortex. Cereb. Cortex 14, 530–542. https://doi.org/10.1093/cercor/bhh015
Hamm, J.P., Yuste, R., 2016. Somatostatin Interneurons Control a Key Component of Mismatch Negativity in Mouse Visual Cortex. Cell Rep. 16, 597–604. https://doi.org/10.1016/j.celrep.2016.06.037
Harris, J.A., Mihalas, S., Hirokawa, K.E., Whitesell, J.D., Choi, H., Bernard, A., Bohn, P., Caldejon, S., Casal, L., Cho, A., Feiner, A., Feng, D., Gaudreault, N., Gerfen, C.R., Graddis, N., Groblewski, P.A., Henry, A.M., Ho, A., Howard, R., Knox, J.E., Kuan, L., Kuang, X., Lecoq, J., Lesnar, P., Li, Y., Luviano, J., McConoughey, S., Mortrud, M.T., Naeemi, M., Ng, L., Oh, S.W., Ouellette, B., Shen, E., Sorensen, S.A., Wakeman, W., Wang, Q., Wang, Y., Williford, A., Phillips, J.W., Jones, A.R., Koch, C., Zeng, H., 2019. Hierarchical organization of cortical and thalamic connectivity. Nature 575, 195–202. https://doi.org/10.1038/s41586-019-1716-z
Henze, D.A., Borhegyi, Z., Csicsvari, J., Mamiya, A., Harris, K.D., Buzsáki, G., 2000. Intracellular Features Predicted by Extracellular Recordings in the Hippocampus In Vivo. J. Neurophysiol. 84, 390–400. https://doi.org/10.1152/jn.2000.84.1.390
Herrera, B., Westerberg, J.A., Schall, M.S., Maier, A., Woodman, G.F., Schall, J.D., Riera, J.J., 2022. Resolving the mesoscopic missing link: Biophysical modeling of EEG from cortical columns in primates. NeuroImage 263, 119593. https://doi.org/10.1016/j.neuroimage.2022.119593
Hosoya, T., Baccus, S.A., Meister, M., 2005. Dynamic predictive coding by the retina. Nature 436, 71–77. https://doi.org/10.1038/nature03689
Hwang, J., Mitz, A.R., Murray, E.A., 2019. NIMH MonkeyLogic: Behavioral control and data acquisition in MATLAB. J. Neurosci. Methods 323, 13–21. https://doi.org/10.1016/j.jneumeth.2019.05.002
Itti, L., Baldi, P., 2009. Bayesian surprise attracts human attention. Vision Res. 49, 1295–1306. https://doi.org/10.1016/j.visres.2008.09.007
Jamali, S., Bagur, S., Brémont, E., Kerkoerle, T.V., Dehaene, S., Bathellier, B., 2024. Parallel mechanisms signal a hierarchy of sequence structure violations in the auditory cortex. https://doi.org/10.1101/2024.08.21.609026
Juavinett, A.L., Nauhaus, I., Garrett, M.E., Zhuang, J., Callaway, E.M., 2017. Automated identification of mouse visual areas with intrinsic signal imaging. Nat. Protoc. 12, 32–43. https://doi.org/10.1038/nprot.2016.158
Kajikawa, Y., Smiley, J.F., Schroeder, C.E., 2017. Primary Generators of Visually Evoked Field Potentials Recorded in the Macaque Auditory Cortex. J. Neurosci. 37, 10139–10153. https://doi.org/10.1523/JNEUROSCI.3800-16.2017
Keller, G.B., Mrsic-Flogel, T.D., 2018. Predictive Processing: A Canonical Cortical Computation. Neuron 100, 424–435. https://doi.org/10.1016/j.neuron.2018.10.003
Kiebel, S.J., Daunizeau, J., Friston, K.J., 2008. A Hierarchy of Time-Scales and the Brain. PLOS Comput. Biol. 4, e1000209. https://doi.org/10.1371/journal.pcbi.1000209
Kok, P., Rahnev, D., Jehee, J.F.M., Lau, H.C., de Lange, F.P., 2011. Attention Reverses the Effect of Prediction in Silencing Sensory Signals. Cereb. Cortex 22, 2197–2206.
Lima, S.Q., Hromádka, T., Znamenskiy, P., Zador, A.M., 2009. PINP: A New Method of Tagging Neuronal Populations for Identification during In Vivo Electrophysiological Recording. PLOS ONE 4, e6099. https://doi.org/10.1371/journal.pone.0006099
Logothetis, N.K., Pauls, J., Augath, M., Trinath, T., Oeltermann, A., 2001. Neurophysiological investigation of

the basis of the fMRI signal. Nature 412, 150–157. https://doi.org/10.1038/35084005
Maier, A., Adams, G., Aura, C., Leopold, D., 2010. Distinct Superficial and Deep Laminar Domains of Activity in the Visual Cortex during Rest and Stimulation. Front. Syst. Neurosci. 4.
Maier, A., Aura, C.J., Leopold, D.A., 2011. Infragranular Sources of Sustained Local Field Potential Responses in Macaque Primary Visual Cortex. J. Neurosci. 31, 1971–1980. https://doi.org/10.1523/JNEUROSCI.5300-09.2011
Maier, A., Tsuchiya, N., 2021. Growing evidence for separate neural mechanisms for attention and consciousness. Atten. Percept. Psychophys. 83, 558–576. https://doi.org/10.3758/s13414-020-02146-4
Maris, E., Oostenveld, R., 2007. Nonparametric statistical testing of EEG- and MEG-data. J. Neurosci. Methods 164, 177–190. https://doi.org/10.1016/j.jneumeth.2007.03.024
Mathis, A., Mamidanna, P., Cury, K.M., Abe, T., Murthy, V.N., Mathis, M.W., Bethge, M., 2018. DeepLabCut: markerless pose estimation of user-defined body parts with deep learning. Nat. Neurosci. 21, 1281–1289. https://doi.org/10.1038/s41593-018-0209-y
McCormick, D.A., Connors, B.W., Lighthall, J.W., Prince, D.A., 1985. Comparative electrophysiology of pyramidal and sparsely spiny stellate neurons of the neocortex. J. Neurophysiol. 54, 782–806. https://doi.org/10.1152/jn.1985.54.4.782
Mehta, A.D., Ulbert, I., Schroeder, C.E., 2000a. Intermodal selective attention in monkeys. I: distribution and timing of effects across visual areas. Cereb. Cortex 10, 343–358. https://doi.org/10.1093/cercor/10.4.343
Mehta, A.D., Ulbert, I., Schroeder, C.E., 2000b. Intermodal Selective Attention in Monkeys. II: Physiological Mechanisms of Modulation. Cereb. Cortex 10, 359–370. https://doi.org/10.1093/cercor/10.4.359
Mendoza-Halliday, D., Major, A.J., Lee, N., Lichtenfeld, M.J., Carlson, B., Mitchell, B., Meng, P.D., Xiong, Y.S., Westerberg, J.A., Jia, X., Johnston, K.D., Selvanayagam, J., Everling, S., Maier, A., Desimone, R., Miller, E.K., Bastos, A.M., 2024. A ubiquitous spectrolaminar motif of local field potential power across the primate cortex. Nat. Neurosci. 27, 547–560. https://doi.org/10.1038/s41593-023-01554-7
Michalareas, G., Vezoli, J., van Pelt, S., Schoffelen, J.-M., Kennedy, H., Fries, P., 2016. Alpha-Beta and Gamma Rhythms Subserve Feedback and Feedforward Influences among Human Visual Cortical Areas. Neuron 89, 384–397. https://doi.org/10.1016/j.neuron.2015.12.018
Miller, E.K., Cohen, J.D., 2001. An integrative theory of prefrontal cortex function. Annu. Rev. Neurosci. 24, 167–202. https://doi.org/10.1146/annurev.neuro.24.1.167
Miller, E.K., Lundqvist, M., Bastos, A.M., 2018. Working Memory 2.0. Neuron 100, 463–475. https://doi.org/10.1016/j.neuron.2018.09.023
Mitchell, J.F., Sundberg, K.A., Reynolds, J.H., 2007. Differential Attention-Dependent Response Modulation across Cell Classes in Macaque Visual Area V4. Neuron 55, 131–141. https://doi.org/10.1016/j.neuron.2007.06.018
Mitzdorf, U., 1985. Current source-density method and application in cat cerebral cortex: investigation of evoked potentials and EEG phenomena. Physiol. Rev. 65, 37–100. https://doi.org/10.1152/physrev.1985.65.1.37
Mitzdorf, U., Singer, W., 1978. Prominent excitatory pathways in the cat visual cortex (A 17 and A 18): A current source density analysis of electrically evoked potentials. Exp. Brain Res. 33, 371–394. https://doi.org/10.1007/BF00235560
Mumford, D., 1992. On the computational architecture of the neocortex. II. The role of cortico-cortical loops. Biol. Cybern. 66, 241–251. https://doi.org/10.1007/BF00198477
Nedungadi, A.G., Rangarajan, G., Jain, N., Ding, M., 2009. Analyzing multiple spike trains with nonparametric granger causality. J. Comput. Neurosci. 27, 55–64. https://doi.org/10.1007/s10827-008-0126-2
Nicholson, C., Freeman, J.A., 1975. Theory of current source-density analysis and determination of conductivity tensor for anuran cerebellum. J. Neurophysiol. 38, 356–368. https://doi.org/10.1152/jn.1975.38.2.356
Nicholson, C., Llinas, R., 1971. Field Potentials in Alligator Cerebellum and Theory of Their Relationship to Purkinje Cell Dendritic Spikes. J. Neurophysiol. 34, 509-+. https://doi.org/10.1152/jn.1971.34.4.509
Ninomiya, T., Dougherty, K., Godlove, D.C., Schall, J.D., Maier, A., 2015. Microcircuitry of agranular frontal cortex: contrasting laminar connectivity between occipital and frontal areas. J. Neurophysiol. 113, 3242–3255. https://doi.org/10.1152/jn.00624.2014
Nourski, K.V., Steinschneider, M., Rhone, A.E., Kawasaki, H., Howard, M.A., Banks, M.I., 2018. Auditory Predictive Coding across Awareness States under Anesthesia: An Intracranial Electrophysiology Study. J. Neurosci. 38, 8441–8452. https://doi.org/10.1523/JNEUROSCI.0967-18.2018

Nowak, L.G., Azouz, R., Sanchez-Vives, M.V., Gray, C.M., McCormick, D.A., 2003. Electrophysiological Classes of Cat Primary Visual Cortical Neurons In Vivo as Revealed by Quantitative Analyses. J. Neurophysiol. 89, 1541–1566. https://doi.org/10.1152/jn.00580.2002

Oostenveld, R., Fries, P., Maris, E., Schoffelen, J.-M., 2011. FieldTrip: Open source software for advanced analysis of MEG, EEG, and invasive electrophysiological data. Comput. Intell. Neurosci. 2011, 156869. https://doi.org/10.1155/2011/156869

Pachitariu, M., Sridhar, S., Stringer, C., 2023. Solving the spike sorting problem with Kilosort. https://doi.org/10.1101/2023.01.07.523036

Pak, A., Kissinger, S.T., Chubykin, A.A., 2021. Impaired Adaptation and Laminar Processing of the Oddball Paradigm in the Primary Visual Cortex of Fmr1 KO Mouse. Front. Cell. Neurosci. 15. https://doi.org/10.3389/fncel.2021.668230

Pfeffer, C.K., Xue, M., He, M., Huang, Z.J., Scanziani, M., 2013. Inhibition of inhibition in visual cortex: the logic of connections between molecularly distinct interneurons. Nat. Neurosci. 16, 1068–1076. https://doi.org/10.1038/nn.3446

Povysheva, N.V., Gonzalez-Burgos, G., Zaitsev, A.V., Kröner, S., Barrionuevo, G., Lewis, D.A., Krimer, L.S., 2006. Properties of Excitatory Synaptic Responses in Fast-spiking Interneurons and Pyramidal Cells from Monkey and Rat Prefrontal Cortex. Cereb. Cortex 16, 541–552. https://doi.org/10.1093/cercor/bhj002

Rao, R. P. N., Ballard, D.H., 1999. Predictive coding in the visual cortex: a functional interpretation of some extra-classical receptive-field effects. Nat. Neurosci. 2, 79–87. https://doi.org/10.1038/4580

Rao, R. P.N, Ballard, D.H., 1999. Predictive coding in the visual cortex: a functional interpretation of some extra-classical receptive-field effects. Nat. Neurosci. 2, 79–87.

Rigotti, M., Barak, O., Warden, M.R., Wang, X.-J., Daw, N.D., Miller, E.K., Fusi, S., 2013. The importance of mixed selectivity in complex cognitive tasks. Nature 497, 585–590. https://doi.org/10.1038/nature12160

Rübel, O., Tritt, A., Ly, R., Dichter, B.K., Ghosh, S., Niu, L., Baker, P., Soltesz, I., Ng, L., Svoboda, K., Frank, L., Bouchard, K.E., 2022. The Neurodata Without Borders ecosystem for neurophysiological data science. eLife 11, e78362. https://doi.org/10.7554/eLife.78362

Sanchez-Vives, M.V., Nowak, L.G., McCormick, D.A., 2000a. Membrane mechanisms underlying contrast adaptation in cat area 17 *in vivo*. J. Neurosci. 20, 4267–4285.

Sanchez-Vives, M.V., Nowak, L.G., McCormick, D.A., 2000b. Cellular mechanisms of long-lasting adaptation in visual cortical neurons *in vitro*. J. Neurosci. 20, 4286–4299.

Schroeder, C.E., Mehta, A.D., Givre, S.J., 1998. A spatiotemporal profile of visual system activation revealed by current source density analysis in the awake macaque. Cereb. Cortex 8, 575–592. https://doi.org/10.1093/cercor/8.7.575

Schultz, W., Dayan, P., Montague, P.R., 1997. A neural substrate of prediction and reward. Science 275, 1593–1599. https://doi.org/10.1126/science.275.5306.1593

Self, M.W., van Kerkoerle, T., Supèr, H., Roelfsema, P.R., 2013. Distinct Roles of the Cortical Layers of Area V1 in Figure-Ground Segregation. Curr. Biol. 23, 2121–2129. https://doi.org/10.1016/j.cub.2013.09.013

Seth, A.K., Suzuki, K., Critchley, H.D., 2012. An interoceptive predictive coding model of conscious presence. Front. Psychol. 3, 395. https://doi.org/10.3389/fpsyg.2011.00395

Siegle, J.H., Jia, X., Durand, S., Gale, S., Bennett, C., Graddis, N., Heller, G., Ramirez, T.K., Choi, H., Luviano, J.A., Groblewski, P.A., Ahmed, R., Arkhipov, A., Bernard, A., Billeh, Y.N., Brown, D., Buice, M.A., Cain, N., Caldejon, S., Casal, L., Cho, A., Chvilicek, M., Cox, T.C., Dai, K., Denman, D.J., de Vries, S.E.J., Dietzman, R., Esposito, L., Farrell, C., Feng, D., Galbraith, J., Garrett, M., Gelfand, E.C., Hancock, N., Harris, J.A., Howard, R., Hu, B., Hytnen, R., Iyer, R., Jessett, E., Johnson, K., Kato, I., Kiggins, J., Lambert, S., Lecoq, J., Ledochowitsch, P., Lee, J.H., Leon, A., Li, Y., Liang, E., Long, F., Mace, K., Melchior, J., Millman, D., Mollenkopf, T., Nayan, C., Ng, L., Ngo, K., Nguyen, T., Nicovich, P.R., North, K., Ocker, G.K., Ollerenshaw, D., Oliver, M., Pachitariu, M., Perkins, J., Reding, M., Reid, D., Robertson, M., Ronellenfitch, K., Seid, S., Slaughterbeck, C., Stoecklin, M., Sullivan, D., Sutton, B., Swapp, J., Thompson, C., Turner, K., Wakeman, W., Whitesell, J.D., Williams, D., Williford, A., Young, R., Zeng, H., Naylor, S., Phillips, J.W., Reid, R.C., Mihalas, S., Olsen, S.R., Koch, C., 2021. Survey of spiking in the mouse visual system reveals functional hierarchy. Nature 592, 86–92. https://doi.org/10.1038/s41586-020-03171-x

Siegle, J.H., López, A.C., Patel, Y.A., Abramov, K., Ohayon, S., Voigts, J., 2017. Open Ephys: an open-source, plugin-based platform for multichannel electrophysiology. J. Neural Eng. 14, 045003. https://doi.org/10.1088/1741-2552/aa5eea

Smout, C.A., Tang, M.F., Garrido, M.I., Mattingley, J.B., 2019. Attention promotes the neural encoding of prediction errors. PLOS Biol. 17, e2006812. https://doi.org/10.1371/journal.pbio.2006812
Solomon, S.S., Tang, H., Sussman, E., Kohn, A., 2021. Limited Evidence for Sensory Prediction Error Responses in Visual Cortex of Macaques and Humans. Cereb. CORTEX 31, 3136–3152. https://doi.org/10.1093/cercor/bhab014
Spratling, M.W., 2010. Predictive coding as a model of response properties in cortical area V1. J. Neurosci. Off. J. Soc. Neurosci. 30, 3531–3543. https://doi.org/10.1523/JNEUROSCI.4911-09.2010
Spratling, M.W., 2008. Reconciling predictive coding and biased competition models of cortical function. Front. Comput. Neurosci. 2, 4. https://doi.org/10.3389/neuro.10.004.2008
Srinivasan, M.V., Laughlin, S.B., Dubs, A., 1982. Predictive coding: a fresh view of inhibition in the retina. Proc. R. Soc. Lond. B Biol. Sci. 216, 427–459. https://doi.org/10.1098/rspb.1982.0085
Supèr, H., Roelfsema, P.R., 2005. Chronic multiunit recordings in behaving animals: advantages and limitations. Prog. Brain Res., Development, Dynamics and Pathiology of Neuronal Networks: from Molecules to Functional Circuits 147, 263–282. https://doi.org/10.1016/S0079-6123(04)47020-4
Tasker, J.G., Hoffman, N.W., Kim, Y.I., Fisher, R.S., Peacock, W.J., Dudek, F.E., 1996. Electrical properties of neocortical neurons in slices from children with intractable epilepsy. J. Neurophysiol. 75, 931–939. https://doi.org/10.1152/jn.1996.75.2.931
Tovar, D.A., Westerberg, J.A., Cox, M.A., Dougherty, K., Carlson, T.A., Wallace, M.T., Maier, A., 2020. Stimulus Feature-Specific Information Flow Along the Columnar Cortical Microcircuit Revealed by Multivariate Laminar Spiking Analysis. Front. Syst. Neurosci. 14.
Tovar, D.A., Westerberg, J.A., Cox, M.A., Dougherty, K., Wallace, M.T., Bastos, A.M., Maier, A., 2023. Near-field potentials index local neural computations more accurately than population spiking. https://doi.org/10.1101/2023.05.11.540026
Trautmann, E.M., Stavisky, S.D., Lahiri, S., Ames, K.C., Kaufman, M.T., O'Shea, D.J., Vyas, S., Sun, X., Ryu, S.I., Ganguli, S., Shenoy, K.V., 2019. Accurate Estimation of Neural Population Dynamics without Spike Sorting. Neuron 103, 292-308.e4. https://doi.org/10.1016/j.neuron.2019.05.003
Uhrig, L., Janssen, D., Dehaene, S., Jarraya, B., 2016. Cerebral responses to local and global auditory novelty under general anesthesia. NeuroImage 141, 326–340. https://doi.org/10.1016/j.neuroimage.2016.08.004
van Kerkoerle, T., Self, M.W., Dagnino, B., Gariel-Mathis, M.-A., Poort, J., Togt, C. van der, Roelfsema, P.R., 2014a. Alpha and gamma oscillations characterize feedback and feedforward processing in monkey visual cortex. Proc. Natl. Acad. Sci. 111, 14332–14341. https://doi.org/10.1073/pnas.1402773111
van Kerkoerle, T., Self, M.W., Dagnino, B., Gariel-Mathis, M.-A., Poort, J., van der Togt, C., Roelfsema, P.R., 2014b. Alpha and gamma oscillations characterize feedback and feedforward processing in monkey visual cortex. Proc. Natl. Acad. Sci. U. S. A. 111, 14332–14341. https://doi.org/10.1073/pnas.1402773111
van Kerkoerle, T., Self, M.W., Roelfsema, P.R., 2017. Layer-specificity in the effects of attention and working memory on activity in primary visual cortex. Nat. Commun. 8, 13804. https://doi.org/10.1038/ncomms13804
Vezoli, J., Vinck, M., Bosman, C.A., Bastos, A.M., Lewis, C.M., Kennedy, H., Fries, P., 2021. Brain rhythms define distinct interaction networks with differential dependence on anatomy. Neuron S0896-6273(21)00725-X. https://doi.org/10.1016/j.neuron.2021.09.052
Wacongne, C., Changeux, J.-P., Dehaene, S., 2012. A Neuronal Model of Predictive Coding Accounting for the Mismatch Negativity. J. Neurosci. 32, 3665–3678. https://doi.org/10.1523/JNEUROSCI.5003-11.2012
Westerberg, J.A., Cox, M.A., Dougherty, K., Maier, A., 2019. V1 microcircuit dynamics: altered signal propagation suggests intracortical origins for adaptation in response to visual repetition. J. Neurophysiol. 121, 1938–1952. https://doi.org/10.1152/jn.00113.2019
Westerberg, J.A., Maier, A., Schall, J.D., 2020. Priming of Attentional Selection in Macaque Visual Cortex: Feature-Based Facilitation and Location-Based Inhibition of Return. eNeuro 7. https://doi.org/10.1523/ENEURO.0466-19.2020
Westerberg, J.A., Schall, J.D., Woodman, G.F., Maier, A., 2023. Feedforward attentional selection in sensory cortex. Nat. Commun. 14, 5993. https://doi.org/10.1038/s41467-023-41745-1
Westerberg, J.A., Schall, M.S., Maier, A., Woodman, G.F., Schall, J.D., 2022. Laminar microcircuitry of visual cortex producing attention-associated electric fields. eLife 11, e72139. https://doi.org/10.7554/eLife.72139
Westerberg, J.A., Sigworth, E.A., Schall, J.D., Maier, A., 2021. Pop-out search instigates beta-gated feature

selectivity enhancement across V4 layers. Proc. Natl. Acad. Sci. 118. https://doi.org/10.1073/pnas.2103702118

Xiong, Y. (Sophy), Donoghue, J.A., Lundqvist, M., Mahnke, M., Major, A.J., Brown, E.N., Miller, E.K., Bastos, A.M., 2024. Propofol-mediated loss of consciousness disrupts predictive routing and local field phase modulation of neural activity. Proc. Natl. Acad. Sci. 121, e2315160121. https://doi.org/10.1073/pnas.2315160121

Xiong, Y. (Sophy), Donoghue, J.A., Lundqvist, M., Mahnke, M., Major, A.J., Brown, E.N., Miller, E.K., Bastos, A.M., 2023. Propofol-mediated loss of consciousness disrupts predictive routing and local field phase modulation of neural activity. https://doi.org/10.1101/2023.09.02.555990

Yan, Y., Zhaoping, L., Li, W., 2018. Bottom-up saliency and top-down learning in the primary visual cortex of monkeys. Proc. Natl. Acad. Sci. U. S. A. 115, 10499–10504. https://doi.org/10.1073/pnas.1803854115

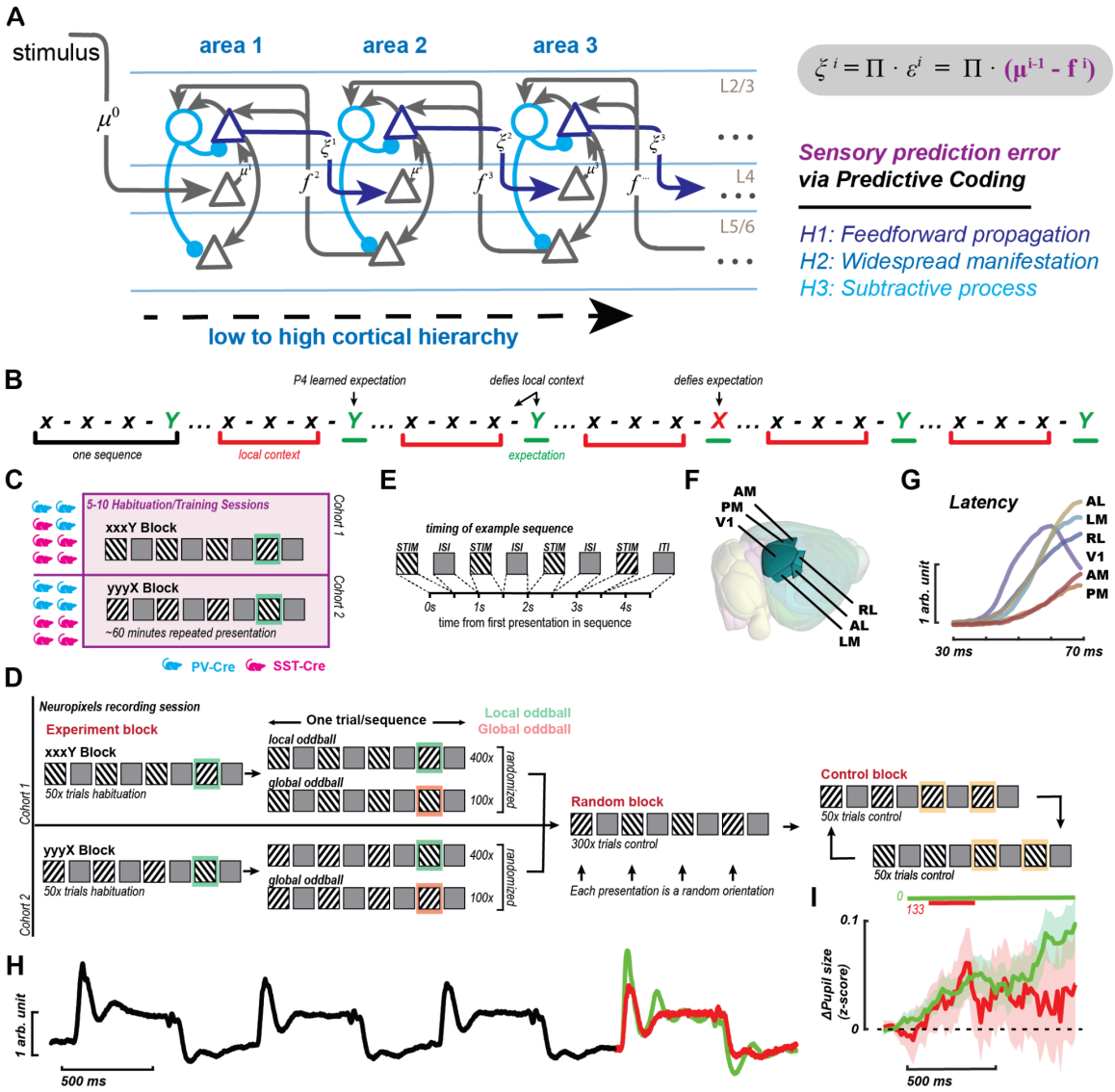

Figure 1. Predictive coding and the global-local oddball experimental paradigm

A. A stimulus enters the system through the excitatory neurons (gray triangles) in the middle input layers of cortex. That ascends the cortical column to the superficial layers (L2/3), excitatory and then inhibitory cells (red circles), before reaching the deep layers (L5/6). The superficial excitatory neurons also innervate the next hierarchical stage of cortical processing (left to right) through the middle input layers. The intracolumnar processing motif then repeats. Crucially, feedback information (with respect to the predictions regarding the stimulus), is sent from deep layers to the superficial layers of the preceding area. The activation from area to area, layer to layer, and cell to cell can be computed from the equation at the top with the terms again indicated in the graphic as to where they are pertinent.
B. Visual stimuli were presented in 4-stimulus sequences consisting of 2-oriented, drifting bar grating, full-screen stimuli (symbolized as 'x'/'X' or 'y'/'Y' where capitalization indicates oddball status).
C. 16 transgenic mice were used in the experiment, genotypes were selected to allow for optotagging of either somatostatin- (magenta) or parvalbumin-positive (cyan) interneurons. Mice were split into 2 training groups, 1 group exposed to xxxY sequences during the entirety of training, 1 group to yyyX.
D. Neuropixels recording sessions were divided into 3 blocks. In the experiment block, mice experienced their trained 'Local' oddball sequence (xxxY or yyyX) for a 50-trial habituation period. Then, on 20% of the next ~500 sequences, they observed a never previously seen 'Global' oddball sequence (xxxX or yyyY). A block of random sequences of 4 stimuli followed the experiment block. A control block followed where alternating sequences of xxxx, yyyy were experienced.
E. Stimuli were presented for 500 ms with a 500 ms inter-stimulus interval and 1 s inter-trial intervals.
F. Neuropixels were introduced into 6 visual cortical regions in all mice (V1, LM, RL, AL, PM, AM).
G. Visual response latencies averaged across all single-units for each visual area followed the expected cascade given visual hierarchical position.
H. Population average response to the 4-stimulus sequences with the global oddball indicated in red and the local oddball in green.
I. Pupil response relative stimulus onset in experiment block showing difference between P4 (oddball) vs. P3 (stimulus prior to oddball) with the global oddball in red and the local oddball in green. Clouds are +/-1 SEM, colored bars at top indicate periods of significant difference.

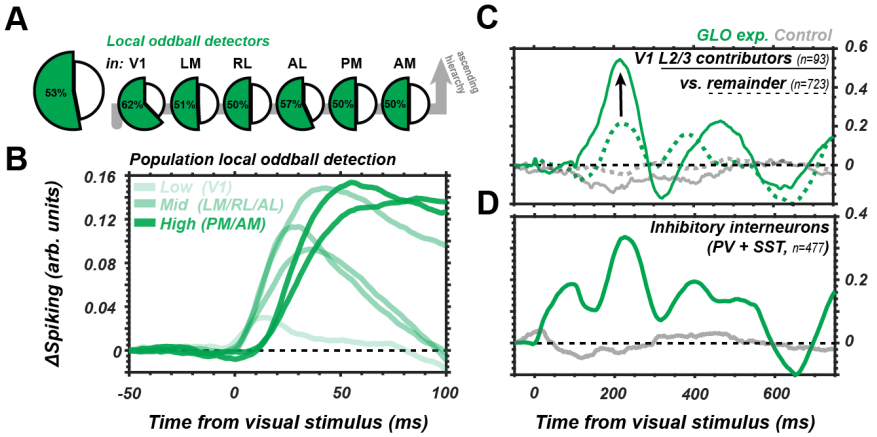

Figure 2. Local oddball responses support experimental predictions of Predictive Coding.

A. Percentage of single-units in an area where a significant detection of the local oddball was found using nonparametric cluster-based permutation testing (see Methods) at the single-unit level.
B. Early period of spiking activation averaged across units for hierarchical area categories (early, light; middle, medium; late, dark green) averaged across single units for a given area. Data area GLO(P4-P3) - CONTROL(P4-P3) demonstrating population enhanced neuronal activation to the local oddball. Detection is later and stronger in higher-order areas.
C. Average response of putative layer 2/3 V1 units to the local oddball (solid green) as compared to the non-layer 2/3 V1 units (dashed green) in the GLO block (P4-P3) and their equivalent responses in the control block (gray solid, gray dashed, respectively). Putative layer 2/3 V1 units have, on average, greater response to the local oddball than other V1 units.
D. Average response of optotagged (see Methods) inhibitory interneurons to the local oddball (green) in the GLO block (P4-P3) and their equivalent response in the control block (gray). Inhibitory interneurons are more active in the oddball condition.

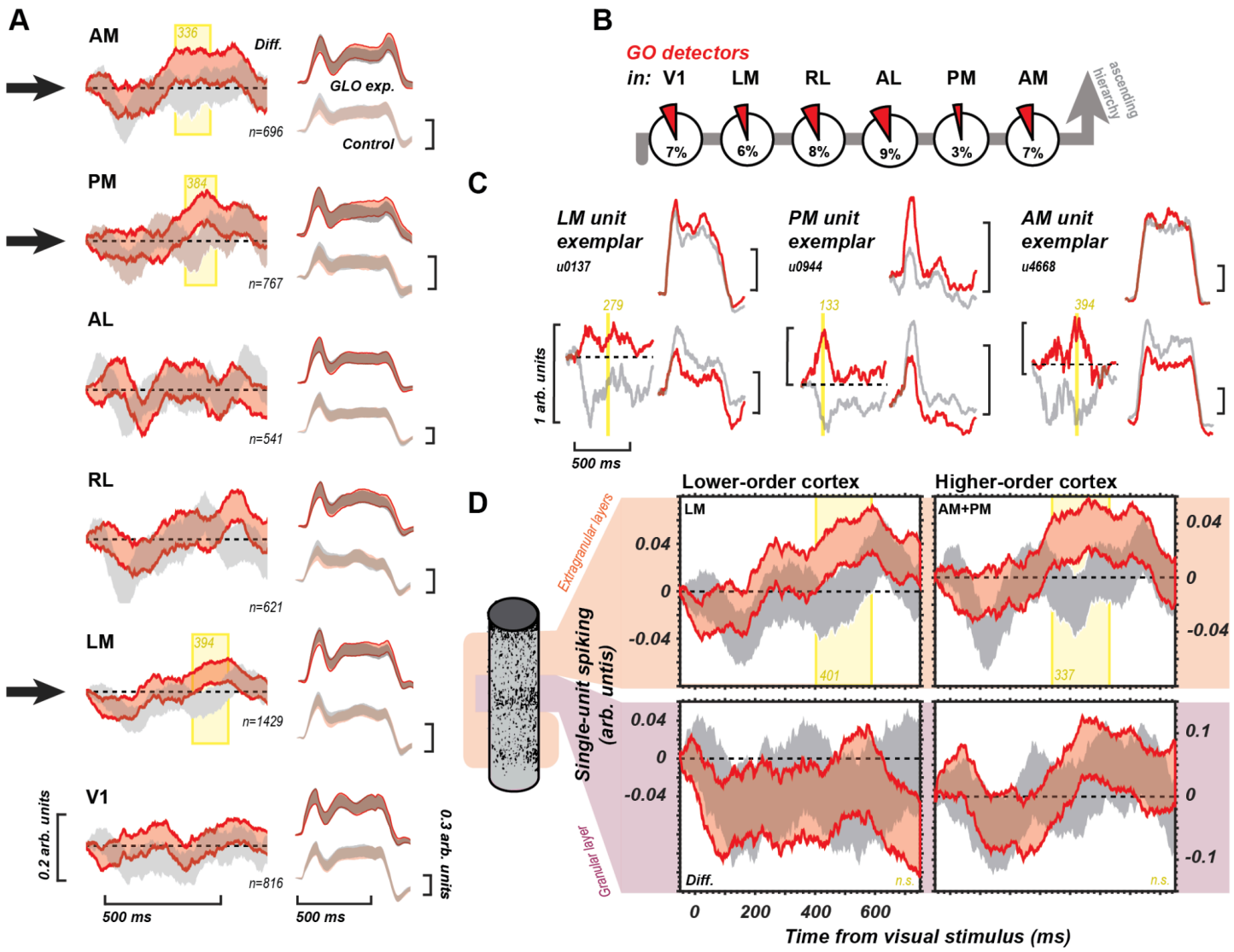

Figure 3. Sparse global oddball detection across visual cortical hierarchy.

A. Global oddball detection across visual cortical areas. Lower-order areas to higher-order areas bottom to top. Clouds are 95% confidence intervals across units in an area. On left, red clouds are P4-P3 in GLO block, gray clouds are P4-P3 in control block. On right, 95% confidence interval clouds for the responses across units per area for the component presentations for the left. Top, GLO experiment with red P4 and gray P3. Bottom, control experiment with red P4 and gray P3. Yellow highlights in LM, PM, AM reflect periods of significant population global oddball detection with the latency indicated.

B. Percentage of single-units in an area where a significant detection of the global oddball was found using nonparametric cluster-based permutation testing (see Methods) at the single-unit level.

C. Single-unit examples of significant global oddball detection in each of the 3 areas that showed significant global oddball detection at the population level. Bottom left of each subpanel shows the P4-P3 difference in the GLO block (red) and control block (gray) with the period of significant detection highlighted in yellow. Right of each subpanel shows the component responses in the GLO block (top) and control block (bottom) for P4 (red) and P3 (gray).

D. Global oddball detection for the areas found to have significant detection at the population level (LM, PM, AM) divided into lower-order (left, LM) and higher-order (right, PM, AM) categories with units further divided by layer. Layer 4 units defined to be in “granular” layer category (purple) and layer 2, 3, 5, and 6 units defined to be in extragranular category (orange). 95% confidence interval clouds plotted identical to panel (A) for P4-P3 differences in each block (red, GLO; gray, control). Yellow highlight indicates period of significant global oddball detection. Significant global oddball detection only present in extragranular layer populations.

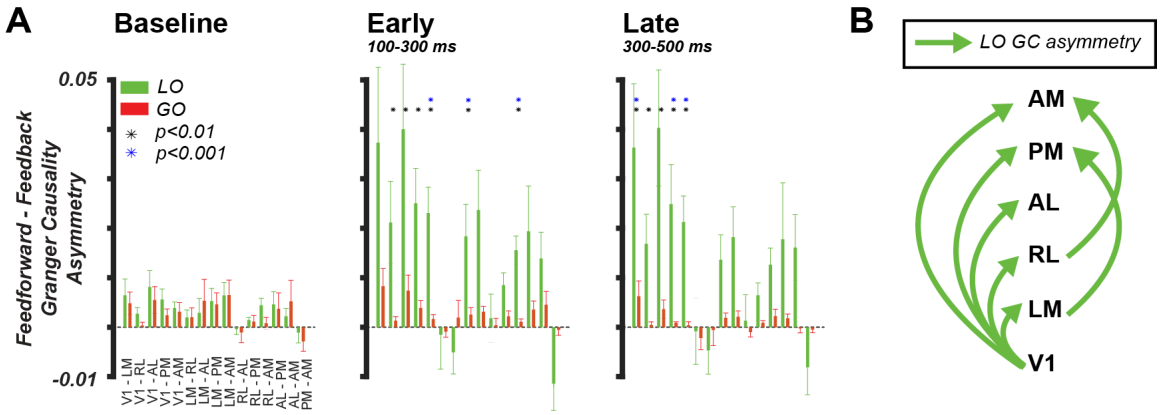

Figure 4. Cortical spiking causalogram for local and global oddballs: Granger causality as a function of time across brain areas.

A. Granger causality asymmetry (Feedforward minus feedback GC) between all possible areas in the baseline (left, pre-oddball time window; middle, initial sensory processing period; right, late sensory processing period).Green bars denote local oddballs, red bars denote global oddballs. Mean across mice, + or - SEM across mice. Asterisks indicate connections that are significantly different from baseline at P<0.01 (black asterisks) and at P<0.001 (blue asterisks).

B. Hierarchical summary of significant changes in GC asymmetry from pre-oddball baseline for local oddballs. Significant interactions at both P<0.01 and P<0.001 are shown, and both early (B) and late (C) time periods are depicted. Global oddballs are not shown because there were no significant observed chances in GC asymmetry.

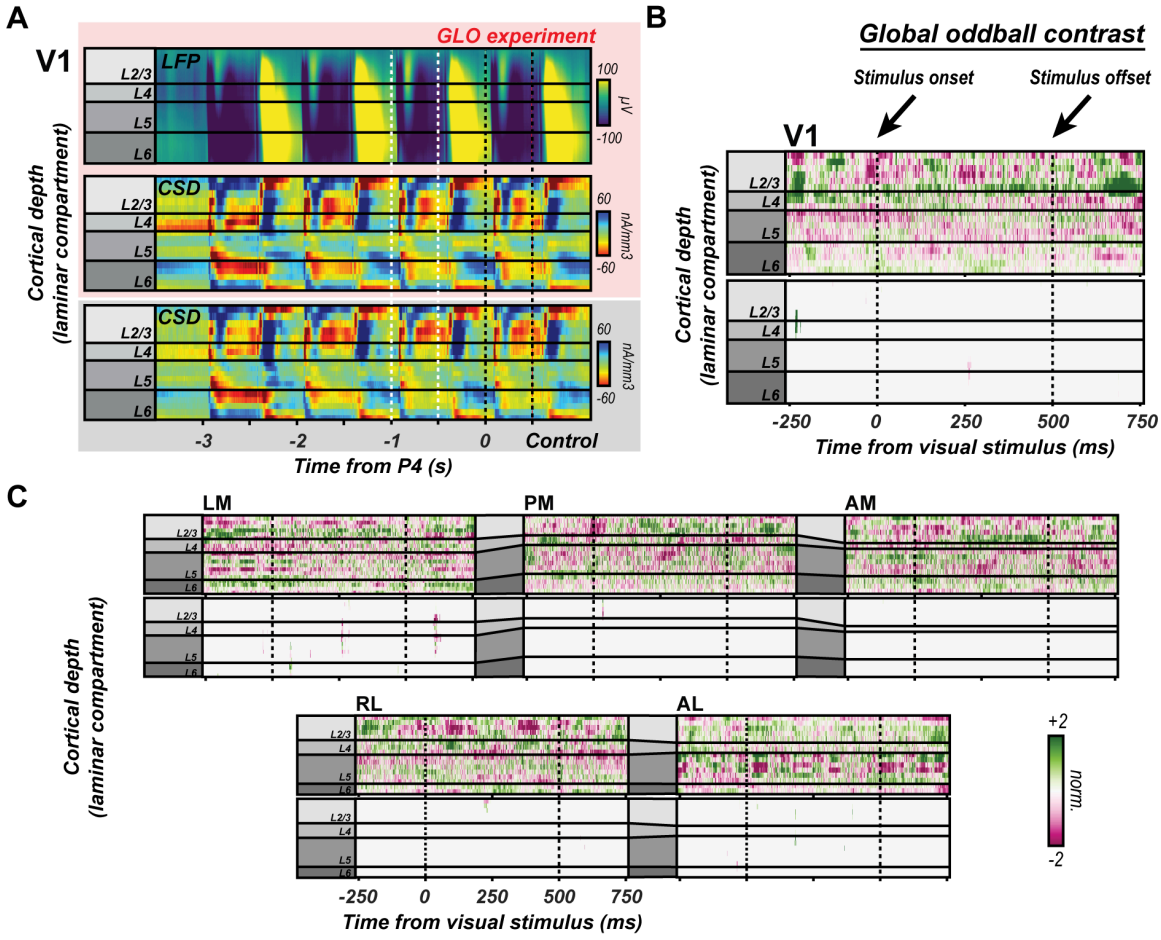

C.

Figure 5. CSD reflecting synaptic activity is not indicative of top-down predictions being fed back to early sensory cortex.

A. Laminar CSD is calculated from the LFP response (top) to sequence presentations averaged across trials and across mice (n=9) for area V1 after aligning cortical depth between animals. CSD is calculated for both the global oddball experimental condition (middle, red highlighted region) and control condition (bottom, gray highlighted region). Epoch between white dotted lines indicates presentation 3, and between the black dotted lines indicates the global oddball presentation (middle) or the presentation 4 in the control (bottom).

B. Evaluating the global oddball contrast for evidence of differences in synaptic activity with global oddball detection in V1. Difference of differences identical to previous global oddball contrasts (P4-P3) for the CSD data. Top image indicates all values following the contrast and normalization between -2 and +2 standard deviations. Bottom image shows the same data with a mask applied to only display significant values (Welch's t-test, $p<0.01$). Color map intensity indicated by scale bar in bottom right of figure.

C. Difference of differences for global oddball contrast for the remaining visual cortical areas. Formatting identical to B.

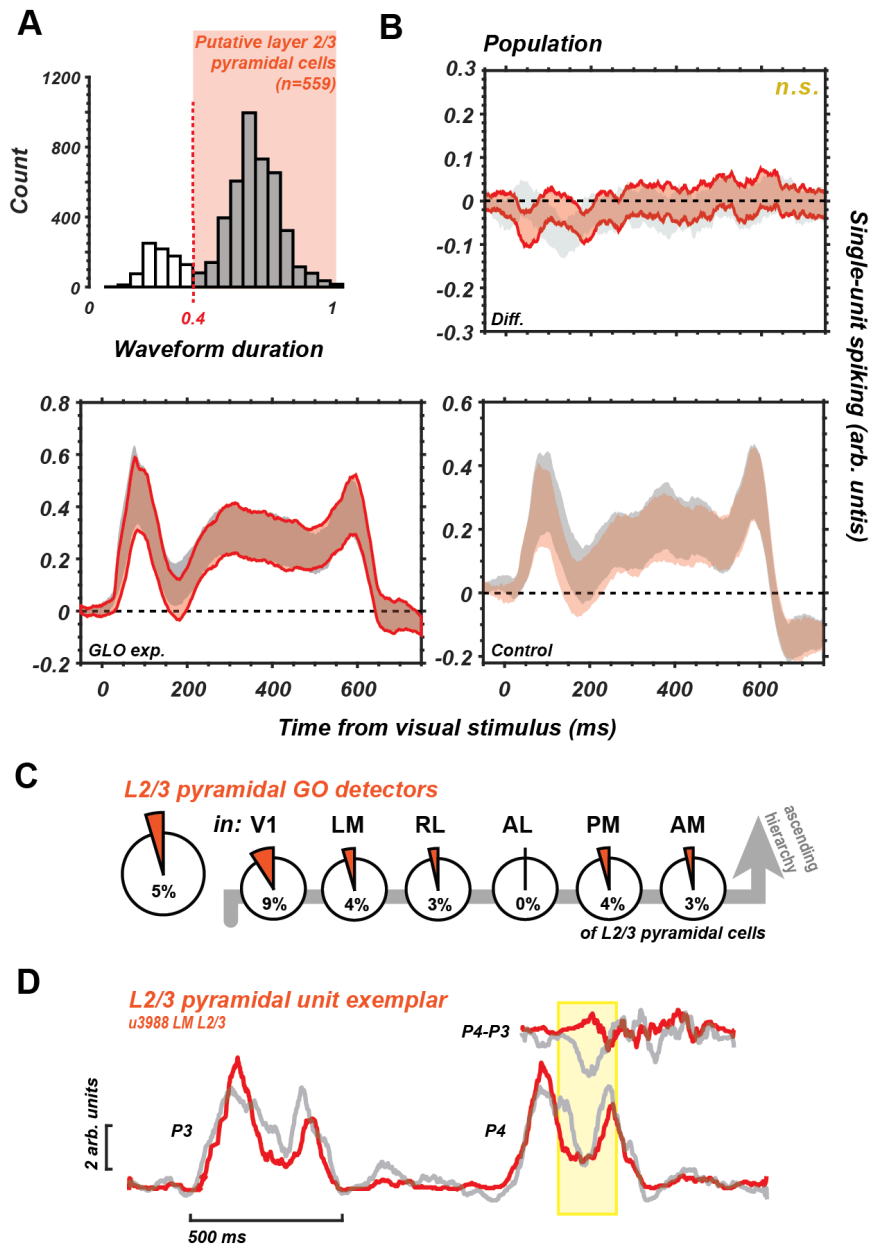

Figure 6. Putative layer 2/3 neurons do not harbor latent feedforward global oddball signals.

A. Histogram of waveform durations of single-units. Threshold for narrow vs. broad spiking neurons set to 0.4 (orange dashed line). Units included as putative layer 2/3 pyramidal cells highlighted in orange, but further reduced by other criteria to obtain final population (see Results).

B. Lack of global oddball detection in layer 2/3 pyramidal cell subpopulation. Clouds are 95% confidence intervals across units. Top right, red cloud is P4-P3 in GLO block, gray cloud is P4-P3 in control block. Bottom, 95% confidence interval clouds for the responses across units for the component presentations for the top right. Left, GLO experiment with red P4 and gray P3. Right, control experiment with red P4 and gray P3.

C. Percentage of specifically putative layer 2/3 pyramidal single-units in an area where a significant detection of the global oddball was found using nonparametric cluster-based permutation testing (see Methods) at the single-unit level.

D. Single-unit example of a putative layer 2/3 unit that was found to have significant global oddball detection. Bottom shows P3 and P4 of the sequence response in the GLO block (red) and control block (gray) with the period of significant detection highlighted in yellow. Above P4 shows the P4-P3 difference for the GLO block (red) vs. the control block (gray) with the yellow highlight reflecting the period of significant detection.

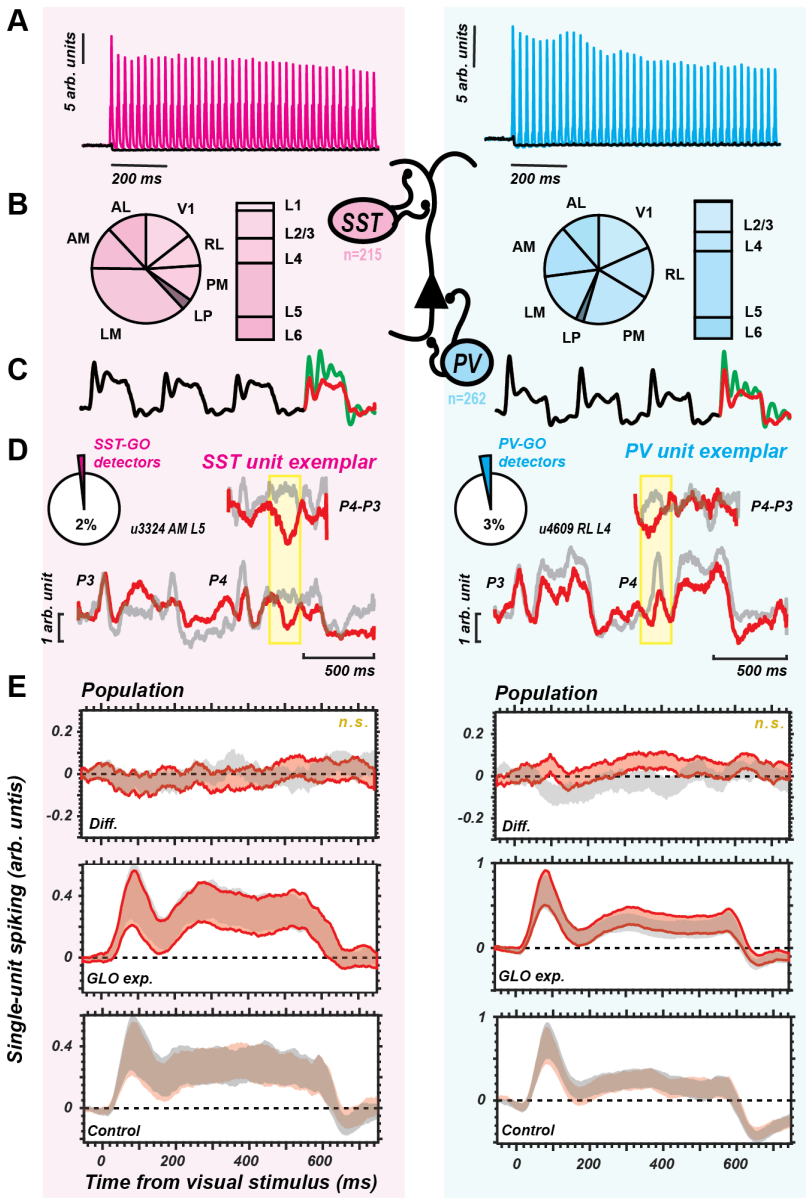

Figure 7. Somatostatin- and parvalbumin-positive interneurons do not follow Predictive Coding models.

A. Response of optotagged SST- (left, magenta, n=215) and PV- (right, cyan, n=262) units as compared to non-optotagged units (black) to 40 Hz laser stimulation in the high power condition (level 1.35) during the optotagging block.
B. Relative proportion of each inhibitory interneuron type across areas (left) and layers (right).
C. Population average response to the oddball sequences for both interneuron types. P1 to P3 in black, local oddball in green, global oddball in red.
D. Percentage of either SST- (left) or PV- (right) tagged interneurons where a significant detection of the global oddball was found using nonparametric cluster-based permutation testing (see Methods) at the single-unit level. Also, example single-unit responses during the sequence presentation (specifically presentations 3 (P3) and 4 (P4)) in the experimental (red) or control (gray) blocks (below) as well as the differences (P4-P3) for those blocks (above). Period of significant difference highlighted in yellow.
E. Lack of global oddball detection in SST and PV cell subpopulations. Clouds are 95% confidence intervals across units. Top, red cloud is P4-P3 in GLO block, gray cloud is P4-P3 in control block. Middle and bottom, 95% confidence interval clouds for the responses across units for the component presentations for the top. Middle, GLO experiment with red P4 and gray P3. Bottom, control experiment with red P4 and gray P3.

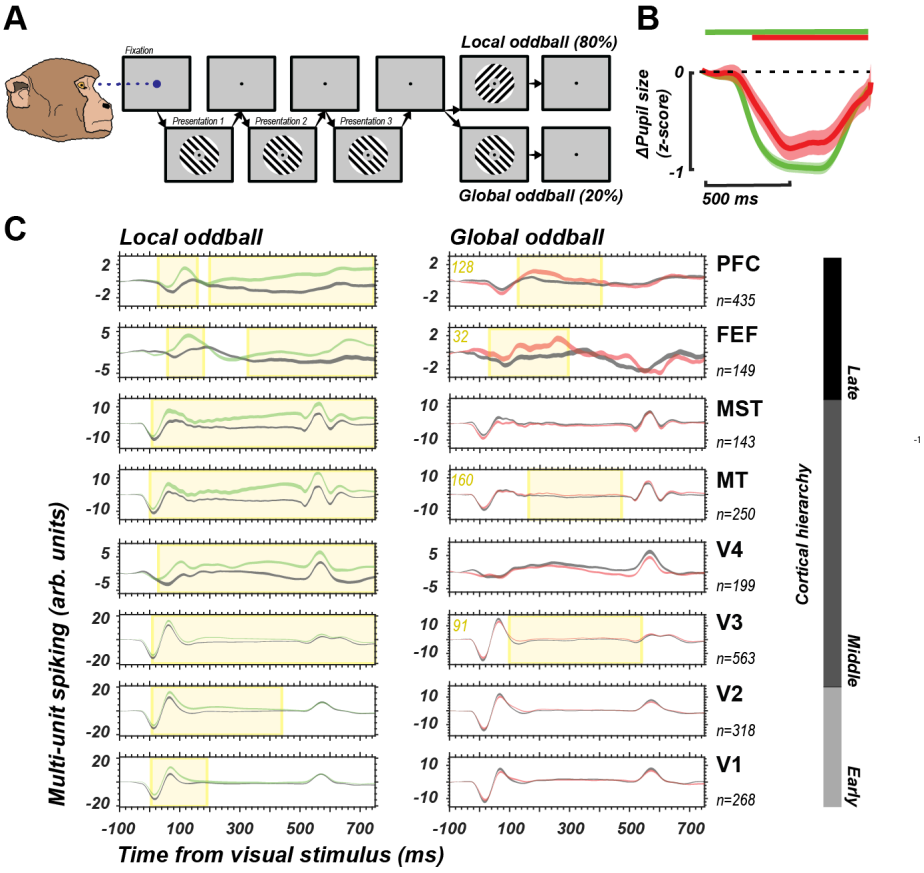

Figure 8. Distinct profiles of local vs. global oddball detection across cortical hierarchy in monkeys.

A. Macaque monkeys (n=2) viewed sequences of drifting grating stimuli while fixating centrally. Sequences were temporally organized identically to the mouse experiment.
B. Pupil response relative stimulus onset showing difference between P4 (oddball) vs. P3 (stimulus prior to oddball) with the global oddball in red and the local oddball in green. Clouds are +/-1 SEM, colored bars at top indicate periods of significant difference.
C. Recordings were performed across 8 brain areas at different stages of the visual cortical processing hierarchy (right). Multi-unit spiking responses were recorded at different sites across multiple recording sessions (n=19). Responses are shown as 95% confidence intervals after performing the same correction as with the mouse data: Green, local oddball - stimulus response prior; Red, global oddball - stimulus previous; Gray, local/global stimulus control - stimulus previous. Yellow highlights indicate periods of significant enhanced oddball activation at the population level.